Research Square

Preprints are preliminary reports that have not undergone peer review.
They should not be considered conclusive, used to inform clinical practice,
or referenced by the media as validated information.

Polygalae Radix processing alleviates the neurotoxicity of Strychni Semen by acting on the tryptophan-kynurenine-serotonin metabolic pathway

Yi Sui[1]
Guizhou University of Traditional Chinese Medicine
Guo Feng[1]
453989352@qq.com
Guizhou University of Traditional Chinese Medicine
Gang Liu[1]
Guizhou University of Traditional Chinese Medicine
Xiaojie Hou[1]
Guizhou University of Traditional Chinese Medicine
Minggang Teng
Guizhou University of Traditional Chinese Medicine
Li Zhang[1]
Guizhou University of Traditional Chinese Medicine
Zhimin Lv[1]
Guizhou University of Traditional Chinese Medicine
Shiqiong Qin[1]
Guizhou University of Traditional Chinese Medicine
Yunli Wei[1]
Guizhou University of Traditional Chinese Medicine
Xinping Wei[1]
Guizhou University of Traditional Chinese Medicine
Wei Li
Guizhou University of Traditional Chinese Medicine
Xiangling Qu
Guizhou University of Traditional Chinese Medicine
Yongyue Gao
Guizhou University of Traditional Chinese Medicine
Qian Qin[4]
Qiandongnan Miao and Dong Autonomous Prefecture Institute of Ethnic Medicine

Jinxi Wang
Qiandongnan Miao and Dong Autonomous Prefecture Institute of Ethnic Medicine
Sibu Ma
Guizhou University of Traditional Chinese Medicine

Research Article

Keywords: Sand-fried Strychni Semen, Polygalae Radix, Polygalae Radix-processed Sand-fried Strychni Semen, Neurotoxicity, Tryptophan metabolic pathway

Posted Date: November 24th, 2026

DOI: https://doi.org/10.21203/rs.3.rs-11262221/v1

License: This work is licensed under a Creative Commons Attribution 4.0 International License.
Read Full License

Additional Declarations: No competing interests reported.

Article

Polygalae Radix processing alleviates the neurotoxicity of Strychni Semen by acting on the tryptophan-kynurenine-serotonin metabolic pathway

Yi Sui[1], Guo Feng[1,2]*, Gang Liu[1], Xiaojie Hou[1], Minggang Teng[1], Li Zhang[1] ,Zhimin Lv[1], Shiqiong Qin[1], Yunli Wei[1], Xinping Wei[1] , Wei Li[1,2], Xiangling Qu[1,3], Yongyue Gao[1,3], Qian Qin[4], Jinxi Wang[4], Sibu Ma[1,5]

1Department of Chinese Materia Medica, Guizhou University of Traditional Chinese Medicine, Guiyang 550025, China.
2Guizhou Inheritance Base of Traditional Chinese Medicine Processing Technology, Guizhou, 3China.Second Affiliated Hospital of Guizhou University of TCM,Guiyang 550000, China.
4Qiandongnan Miao and Dong Autonomous Prefecture Institute of Ethnic Medicine, Kaili City, Guizhou Province, 556000, China.
5Guizhou Key Laboratory of Miao Medicine, Guiyang 550025, China.
*Corresponding author: Guo Feng: 453989352@qq.com.

Abstract

Background: Sand-fried Strychni Semen(SSS) is a traditional Chinese medicinal herb with the effects of dredging collaterals to relieve pain, dissipating stagnation and reducing swelling. However, it is highly toxic and it's active constituents overlap with a narrow therapeutic window, which easily leads to poisoning, and long-term administration is not recommended. In Chinese ethnic medicine, Polygalae Radix(PR) water decoction has been used as a remedy for SSS induced poisoning, with remarkable detoxification effects. This folk therapy has been widely applied by local practitioners, yet the underlying mechanism by which PR relieves SSS poisoning remains unclear. Before clinical use, Chinese herbal medicines are usually subjected to processing to enhance efficacy and reduce toxicity. Therefore, this study aims to explore whether processing SS with PR can attenuate the toxicity of SSS.

Purpose: A method for processing SSS using PR decoction as an excipient was designed, its detoxification effect was observed, and the underlying detoxification mechanism was explored.

Methods: First, SSS was prepared after being processed with PR decoction. Liquid chromatography-mass spectrometry (LC-MS) was adopted to compare the composition changes and transformation rules of SSS before and after PR processing, and to determine the content variations of its toxic components, strychnine and brucine. Subsequently, an acute toxicity test in mice was carried out to compare the LD_{50} values of SSS before and after PR processing, evaluating the anti-inflammatory and analgesic effects of PR-SSS under optimal processing conditions on mice. So as to observe and verify the toxicity-attenuating and efficacy preservation effect of Polygalae Radix-processed Sand-fried Strychni Semen (PR-SSS). A sub-chronic toxicity experiment was then performed in rats to compare the neurotoxicity of SSS and PR-SSS. Differences in neurotoxicity were evaluated based on rat behavioral tests and brain histopathological examination. Metabolomics and transcriptomics technologies were used to detect brain-tissue samples from rats treated with SSS and PR-SSS. Differentially expressed metabolites and genes were screened out, and key pathways related to detoxification were enriched. Key neurotransmitters in rat brain tissues were further measured to validate the function of the enriched pathways. Finally, molecular docking was conducted between the newly-generated compounds in

PR-SSS and key target proteins of the validated pathways, to clarify the potential correspondence between these new constituents and the targets of toxicity-attenuating pathways.

Results: After processing with PR, the contents of the key toxic constituents strychnine and brucine in SSS decreased by 36.23% and 35.62%, respectively. PR-SSS contained 17 original constituents derived from SSS, together with 77 newly-appeared compounds. Among these newly-formed substances, 64 were prototype components originating from PR, and the remaining 13 were newly-generated compounds transformed from constituents presented in SSS and PR. The related reactions involved hydrolysis, condensation, oxidation and other chemical transformations. In terms of toxicity, the LD50 value of PR-SSS for acute toxicity in mice increased by 42.24 % compared with SSS. PR-SSS significantly reduced the number of pain writhing in mice (P<0.05), markedly increased their pain threshold (P<0.05), and significantly attenuated ear swelling in mice with inflammation (P<0.05); in some experimental groups, its anti-inflammatory and analgesic effects were significantly greater than those observed with SSS at the same dose (P<0.05). PR-SSS significantly shortened the time taken by poisoned rats to cross the balance beam (P<0.05), markedly increased the total travel distance in the open-field test (P<0.05), and effectively alleviated the neurotoxic symptoms induced by SSS in rats. Brain histopathological observations revealed pathological lesions and reduced Nissl bodies in the hippocampus of rats in the SSS group, whereas these injuries were ameliorated in the PR-SSS group. Metabolomic and transcriptomic analyses on rat brain tissues demonstrated that the significantly enriched differential metabolic pathway between the PR-SSS and SSS groups was the tryptophan metabolic pathway, which was the common pathway enriched by differential metabolites and genes from both omics data. Neurotransmitter determination in brain tissues further confirmed the changes of key neurotransmitters in this pathway. Molecular-docking results indicated that five newly-generated compounds, namely Oliveramine, Scroneoside A, Cimicifugamide, Picrasidine C and Compound 11, exhibited favorable binding activities with the key target proteins in the tryptophan metabolic pathway. These compounds might serve as the critical active constituents responsible for the detoxification effect of PR-SSS.

Conclusion: PR-SSS can reduce the contents of toxic constituents in SSS and generate several new effective toxicity-attenuating components. These components mainly act via the tryptophan-kynurenine-serotonin metabolic pathway, alleviate central neurotoxic injury induced by SSS by regulating the levels of neurotransmitters related to neurotoxicity and neuroprotection.

Keywords: Sand-fried Strychni Semen; Polygalae Radix; Polygalae Radix-processed Sand-fried Strychni Semen; Neurotoxicity; Tryptophan metabolic pathway

1. Introduction

Strychni Semen(SS) is the dried ripe seed of Strychnos nux-vomica L., a plant belonging to the genus Strychnos of the family Loganiaceae. It exerts the effects of dredging collaterals to relieve pain, dissipating stagnation and reducing swelling but with highly toxic. Clinically, it is mainly used for the treatment of traumatic injuries, swelling and pain caused by fractures, intractable rheumatism, numbness and paralysis, carbuncles and sores, sore throat and other symptoms[1]. As a traditional Chinese medicinal herb, SS was first recorded in Compendium of Materia Medica written by Li Shizhen in the Ming Dynasty and has a long-standing history of medicinal application. More than 200 well-known

ancient and modern prescriptions contain this herb, among which prescriptions for bi-syndrome (arthralgia-syndrome) and traumatic disorders account for approximately 70 % [2] .Known as "the king of herbs for dredging collaterals and relieving pain", SS is a toxic medicinal material. Nevertheless, there is a classical viewpoint that “medicinal substances treat diseases by virtue of their toxicity”. Modern pharmacological studies have demonstrated that SS possesses multiple pharmacological activities, including anti-inflammatory and analgesic effects, promotion of bone-tissue healing, nerve-repair-promoting action, anti-arrhythmia and anti-tumor activities [3].Nevertheless, SS is “highly toxic” with violent poisonous effects. It exerts toxic impacts on the central nervous system, cardiovascular system, digestive system and urinary system, and its principal toxicity targets the central nervous system [4]. Its acute toxic symptoms are mainly manifested as dizziness, headache, irritability, lip cyanosis, muscle twitches and psychiatric disorders. Severe cases may present with loss of consciousness, risus sardonicus, trismus, dyspnea, nuchal rigidity, opisthotonus, and urinary and fecal incontinence [5].The therapeutic dose of SS is close to its toxic dose, accompanied by considerable individual variation. It is also characterized by rapid absorption, short latency period of intoxication, acute and severe symptoms, and a poor prognosisp [6]. Its narrow scope of application and narrow therapeutic window, along with the inadvisability of long-term administration, greatly limit the exertion of its pharmacological effects and compromise its medication safety. Ancient and modern physicians commonly reduce the toxicity of SS through processing and compatibility. The Sand-fried method is recommended as the processing technique for SS in the 2025 edition of Chinese Pharmacopoeia [1].However, although the contents of strychnine and brucine in Sand-fried Strychni Semen（SSS） are decreased, it still retains considerable toxicity to preserve its therapeutic efficacy. Therefore, finding an approach that can reduce the toxicity of SSS while retaining its efficacy has become an urgent problem to be solved for improving its clinical safety.

At present, there is no effective solution for SSS induced poisoning. Nevertheless, according to the medication experience of ethnic minority areas in Guizhou China, the decoction of PR is commonly used to rescue SSS poisoning with remarkable detoxification effects, which provides us with important inspiration. Two research questions are accordingly put forward: Firstly, what is the underlying mechanism by which PR alleviates SSS poisoning? Secondly, is it feasible to develop a processing method using PR as an auxiliary material for the processing of SSS, so as to improve its medication safety at the source of administration, rather than implementing rescue measures after toxic reactions occur?

Therefore, this study designed a processing method for SSS using PR as an auxiliary material, and experiments were performed to verify its remarkable detoxification effect, especially against neurotoxicity. Metabolomics was adopted to explore the signaling pathways underlying its central detoxification effect. Furthermore, transcriptomics was used to identify the key factors involved in these pathways. This study aims to develop a novel strategy to improve the medication safety of SSS and elucidate the mechanism by which PR alleviates the neurotoxicity of SSS.

2. Materials and Methods

2.1. Main materials and instrumentation

Liquid chromatography-time-of-flight mass spectrometry system (Waters G2-XS Q-ToF); Waters Traditional Medicine Library Version 2.0; Tracker animal trajectory analysis software; paraffin-embedding machine; microtome; image acquisition system; Q Exactive HF-X mass spectrometer (Thermo Scientific); Vanquish ultra-high-performance liquid chromatograph (Thermo Scientific); Centrifuge 5424R (Eppendorf); QTRAP 6500 LC-MS/MS system (SCIEX), etc. SPF Kunming (KM) male mice, weighing 18–22 g, SPF SD male rats were purchased from Chongqing Tengxin Biotechnology Co., Ltd. (Animal

Experimentation License No.: SCXK (Yu) 2024-0005, SCXK (Yu) 2025-0007). The housing environment was well-ventilated, with a temperature of 22–25 °C and a relative humidity of 50%–60%. All animals in each group were allowed free access to food and water; after 3 days of acclimatization, the experiments were initiated. All experimental procedures complied with the animal experimentation ethics guidelines of Guizhou University of Traditional Chinese Medicine (Ethics Application No.: 20241118002).

2.2. Preparation of SSS and PR-SSS

2.2.1. Preparation of SSS decoction pieces and their water decoction (1 g/mL, 100 mL)

100 g of crude SSS was soaked in water for 3 d for full softening. The softened SSS was cut into 3 mm × 3 mm thick slices, dried at 40 °C, and stored at room temperature for later use. Subsequently, 100 g of the above-mentioned decoction pieces were ground into coarse particles, then 800 mL of water was added, and the mixture was decocted under reflux for 2 h before filtration. The residue was added with 500 mL of water and decocted under reflux again for 1 h, followed by filtration. The two filtrates were combined and concentrated by evaporation to 100 mL, yielding 100 mL of SSS water decoction with a concentration of 1 g/mL. The decoction was stored in a refrigerator at 4 °C until use.

2.2.2. Preparation of PR juice (2.5 g/mL, 110 mL; 1 g/mL, 100 mL)

375 g of crude de-cored PR material was added to 3000 mL of water and decocted in an induction cooker pot for 2 h, followed by filtration. The residue was supplemented with 1800 mL of water and decocted in the induction cooker pot for another 1 h before filtration. The two filtrates were combined and concentrated by evaporation with continuous stirring. A total of 150 mL of PR decoction at a mass concentration of 2.5 g/mL was obtained. Then, 40 mL of this decoction was mixed with 60 mL of water to prepare 100 mL of 1 g/mL PR juice. Finally, 110 mL of 2.5 g/mL PR water decoction and 100 mL of 1 g/mL PR decoction were acquired and stored in a refrigerator at 4 °C for subsequent experiments.

2.2.3. Preparation of PR-SSS decoction pieces and their water decoction (1 g/mL, 100 mL)

100 g of SSS was soaked in water for 3 d to achieve full softening. The softened SSS was cut into 3 mm × 3 mm thick slices, dried at 40 °C, and preserved at room temperature for standby. The sliced SSS pieces were mixed thoroughly with 100 mL of the above-prepared 2.5 g/mL PR juice. The mixture was boiled over high-heat flame until nearly dry, then the heat was turned off. Residual heat inside the pot was used for further drying so that all the PR juice adhered to the SSS slices without residual liquid left in the pot. The obtained PR-SSS pieces were taken out, cooled to room temperature, dried at 40 °C, stored at room temperature. Afterwards, 100 g of the above-prepared PR-SSS pieces were ground into coarse particles and completely transferred into a round-bottom flask. After adding 800 mL of water and mixing well, the mixture was decocted under reflux for 2 h and filtered. The residue was mixed with 500 mL of water and decocted under reflux once more for 1 h, followed by filtration. The two filtrates were combined and concentrated to obtain 100 mL of water decoction of PR-SSS with a mass concentration of 1 g/mL. The finished decoction was stored in a refrigerator at 4 °C for later use.

2.3. Component testing of SSS and PR-SSS

The components of SSS, PR-SSS and PR decoctions were analyzed by HPLC-QTOF/MS. Chromatographic conditions: Waters HClass high-performance liquid chromatography system. Chromatographic column: Waters BEH C18 column (50 mm × 2.1 mm, 1.7 μm). Mobile phase A: 0.1% formic acid in water; Mobile phase B: acetonitrile containing 0.1% formic acid. The elution procedure is shown in Table 1. Injection volume: 2 μL; flow rate: 0.4 mL/min; column temperature: 40 °C; detection wavelength: 420 nm.

Table 1. HPLC-QTOF/MS Elution Gradient Program

Time/min	Flow rate/（mL/min）	A / %	B / %
0.0	0.4	95	5
1.0	0.4	95	5
35.0	0.4	2	98
37.0	0.4	2	98

37.1	0.4	95	5
40.0	0.4	95	5

Mass-spectrometry conditions: Liquid chromatography-time-of-flight mass spectrometry system (Waters G2-XS Q-ToF). Data were acquired in both positive and negative electrospray ionization (ESI) modes. Capillary voltage: 2 kV; source temperature: 110 °C; desolvation temperature: 400 °C; desolvation gas (nitrogen) flow rate: 800 L/h; mass scan range: 50–2000 m/z; collision energy: 20–40 V.

Chemical constituents in each sample were identified using the Waters Traditional Medicine Library Version 2.0 (containing information on all herbal medicines listed in the 2025 edition of Chinese Pharmacopoeia as well as 6400 compounds related to these herbs). The transformation rules of the newly-generated chemical components were further analyzed.

2.4. Acute toxicity test on mice

Kunming(KM) mice were divided into two groups: the SSS decoction group and the PR-SSS decoction group. In the preliminary acute-toxicity test, the maximum non-lethal dose (D_n) and the minimum fully-lethal dose (D_m) of the two groups were obtained, which were used as the upper and lower dose limits for each group in the formal acute-toxicity experiment. Subsequently, the dose ratio between groups and the administration dose of each subgroup were determined according to the formula: $\sqrt[n-1]{Dm/Dn}$.

Another 120 KM mice were divided into the SSS decoction group and the PR-SSS decoction group. Each main group was subdivided into six subgroups, with 10 mice in each subgroup. The drug solutions were prepared in advance and diluted to the corresponding concentrations. The administration concentration was calculated according to the formula: Administration concentration = Administration dose / Administration volume. The administration volume for all groups was 10 mL/kg. After single intragastric administration, the toxic symptoms of mice were observed. The number of dead mice within 7 days was recorded, and the mortality rate was calculated. The LD_{50} value of each group was determined by the modified Karber's method. The formula is shown as formula (1).

$$\lg(LD_{50})=X_m-i(\sum p-0.5) \quad (1)$$

Note: X_m: logarithm of the maximum dose; i: difference between the logarithms of adjacent doses; p: mortality rate of each dose group (expressed as 0–1).

2.5. Anti-inflammatory and analgesic assay on mice

2.5.1. Assessment of the analgesic effect of PR-SSS combined with SSS using the acetic acid writhing test

Male Kunming (KM) mice were randomly assigned to the following groups: Control group (administered saline), Low-dose group (25 mg/kg), Medium-dose group (50 mg/kg), and High-dose group (75 mg/kg) receiving SSS decoction; Low-dose group (25 mg/kg), Medium-dose group (50 mg/kg), and High-dose group (75 mg/kg) receiving PR-SSS decoction (Dose is calculated based on the quality of SSS); and Aspirin group (20 mg/kg), as the active drug group. With seven mice in each group. Administration was performed via oral gavage at a dose of 10 mL/kg for 3 days; the analgesic efficacy of each group was evaluated using the acetic acid writhing test following the final administration on the third day. The experimental environment was maintained at approximately 20℃. A 0.5% acetic acid aqueous solution (0.2 mL per mouse) was administered via intraperitoneal injection; the writhing response typically emerges within 2 minutes and reaches its peak frequency after 15 minutes. Therefore, the number of writhing episodes in mice was observed and recorded within 15 minutes post-administration. The analgesic rate was calculated as:

[(Number of writhing episodes in control group - Number of writhing in the treated group) / Number of writhing in the control group] × 100%.

2.5.2. Assessment of the analgesic effect of PR-SSS decocted with SSS decocted using the hot plate method

Fifty female KM mice were subjected to a baseline pain threshold screening; mice with a latency period of less than 5s or greater than 30s were excluded. The remaining mice were grouped and administered the drug according to the method described in front, with continuous administration for 3 days. After the final administration, the mice were placed in a beaker placed on a water bath maintained at 55±0.5℃; the time (s) at which the mice first exhibited the post-lateral paw licking response was observed and recorded as the pain latency period. The maximum observation time was set at 60s; any duration exceeding 60s was recorded as 60s. Prior to drug administration, the baseline pain thresholds for each group were measured and recorded; the values were averaged based on two measurements taken at 5-minute intervals. After the final administration, the pain latency period (s) of the mice in each group was measured and recorded at 30,60,90, and 120 minutes post-administration, with measurements rounded to two decimal places.

2.5.3. Xylene-induced ear swelling experimental study on the anti-inflammatory effect of PR-SSS and SSS

42 male KM mice were grouped and administered the drug according to the method described in front; administration was carried out for 3 days. Following the last administration, the mice were lightly anesthetized with ether, and xylene was applied uniformly to the surface of their right ears (20 μL per mouse); the left ears were left untreated. After 3 h, the mice from each group were sacrificed, and ear tissues from both the left and right at the designated fixation points were harvested using a 6 mm punch. The mass of each ear (mg) was measured, and the ear swelling degree was calculated as follows:

Ear swelling degree (mg) = Mass of the inflamed ear (mg) - Mass of the non-inflamed ear (mg).

2.6. Subchronic central toxicity on SD rats

2.6.1. Animal's administration of SSS and PR-SSS

Sprague-Dawley (SD) rats were randomly divided into the normal group(NG), SSS groups (low-70 mg/kg, medium-210 mg/kg and high-dose 350 mg/kg, L, M, H), PR-SSS groups (low-70 mg/kg, medium-210 mg/kg and high-dose 350 mg/kg, L, M, H, based on the quality of SSS decoction pieces), and the PR group, with 10 rats in each group. Among them, 70 mg/kg(L) was the upper-limit clinical dose specified in the Chinese Pharmacopoeia, 210 mg/kg(M) was three-fold of this upper-limit dose, and 350 mg/kg(H) was five-fold of this upper-limit dose. Rats in each group were administered the corresponding drugs for 15 consecutive days. The beam-walking test and open-field test were performed on day 14 of administration. After the last administration, blood samples were collected from the abdominal aorta. All rats were sacrificed, and brain tissues were harvested for pathological examination and omics analysis.

2.6.2. Beam walking and open field testing

Rats in each group have beam-walking training for 3 days in advance. Successful training was defined as rats crossing the beam within 5 s. Animals that failed to meet this criterion received additional training sessions, with at least three trials per day for three consecutive days. The formal beam-walking test was performed on day 14 of drug administration. The traversal time was recorded precisely from the moment the fore-paws stepped onto the beam until the hind-paws left the beam. The test was carried out without any manual assistance. Behavioral detection started 15 min after intragastric administration. If a rat stayed motionless on the beam or fell off while attempting to cross, the traversal time was recorded as 30 s. Any crossing time longer than 30 s was capped at 30 s.

The open-field box for rats was 1 m in length, 1 m in width and 40 cm in height, with a black-painted bottom. A digital camera was installed 2 m directly above the box, whose field-of-view covered the entire interior of the open-field arena. The open-field test was performed on day 14 of administration in a quiet environment. Each rat was placed at the central area of the box bottom, and video recording and timing were started simultaneously. Continuous observation and video acquisition lasted for 5 min. The interior and bottom surface of the box were cleaned between trials before testing the next animal. The total movement distance, average movement speed, number of entries into the central circle and residence time in the central

zone of rats were recorded. Videos of each rat were saved in MP4 format. Four rats from each group were selected for video recording. All behavioral tests began 15 min after intragastric administration.

2.6.3. Histopathological investigation

Rats in each group were sacrificed after the last administration, and brain tissues were collected for pathological examination. The brain tissues were immersed in 4 % paraformaldehyde for 24 h for fixation. After gradient dehydration with ethanol, the tissues were embedded in paraffin and sectioned. The sections of each group were stained using a hematoxylin-eosin (HE) staining kit and a Nissl body staining kit respectively, and all experimental procedures were performed in accordance with the manufacturer's instructions. Pathological changes and Nissl-body staining of the sections were observed and analyzed under a microscope.

2.7. Cerebral tissue metabolomics

2.7.1. Sample collection

Samples were thawed on ice after removal from the -80 °C freezer (all subsequent operations were performed on ice). The samples were ground thoroughly under liquid-nitrogen conditions. Approximately 20 mg of each ground sample was transferred into a correspondingly numbered centrifuge tube, followed by the addition of 400 μL of 70 % aqueous methanol extraction solution containing internal standard. The mixture was vortex-shaken at 1500 r/min for 5 min and incubated on ice for 15 min. After centrifugation at 12 000 r/min for 10 min at 4 °C, 300 μL of the supernatant was transferred into another correspondingly numbered centrifuge tube and kept at −20 °C for 30 min. A second centrifugation was carried out at 12 000 r/min for 3 min at 4 °C. Finally, 200 μL of the resulting supernatant was transferred into an insert liner of the corresponding sample vial for instrumental analysis.

2.7.2. Metabolomics analysis

2.7.2.1. Chromatographic conditions

Chromatographic separation was performed on a Waters ACQUITY Premier HSS T3 Column (1.8 μm, 2.1 mm × 100 mm). Mobile phase A consisted of 0.1 % formic acid in water, and mobile phase B was 0.1 % formic acid in acetonitrile. The column temperature was set at 40 °C, the flow rate was 0.4 mL/min, and the injection volume was 3 μL. The gradient elution program is shown in Table 2.

Table 2. Chromatographic separation Elution Gradient Program

Time/min	Flow rate/（mL/min）	A / %	B / %
0.0	0.4	95	5
2.0	0.4	80	20
5.0	0.4	40	60
6.0	0.4	1	99
7.5	0.4	1	99
7.6	0.4	95	5
10.0	0.4	95	5

2.7.2.2. Mass spectrometric conditions

Vaporizer temperature: 350 °C (ESI^+)/650 °C (ESI^-); Ion transfer tube temperature: 320 °C; Scan Range (m/z): 70-1000.

2.8 Cerebral tissue transcriptomics

RNA extraction and purification: Approximately 50 mg of brain tissue was collected, and 1 mL of Trizol reagent was added per 50 mg tissue. The tissue was fully homogenized on ice using a homogenizer. After centrifugation, 200 μL of the

supernatant was transferred, and 500 μL of isopropanol was added to precipitate RNA. The RNA pellet was washed thoroughly three times with 75 % ethanol and finally dissolved in 100 μL of DEPC-treated water for subsequent use.

RNA purity detection, concentration calculation and dilution: The purity of RNA was determined with an ultraviolet-visible spectrophotometer. RNA samples with an A260/A280 ratio > 1.7 were regarded as qualified. The mass concentration of RNA (mg/L) was calculated as: RNA concentration = A260 × 40. According to the measured RNA concentration, the RNA sample was diluted with DEPC-treated water to prepare 50 μL of RNA working solution at 200 mg/L for later use.

Reverse transcription: A total of 6 μL of diluted RNA solution was reverse-transcribed into complementary DNA (cDNA) following the manufacturer's instructions of the High-Capacity Reverse Transcription Kit. The cDNA product was diluted with DEPC-treated water to a final concentration of 10 mg/L. Reverse-transcription reaction conditions were set as follows: 25 °C for 10 min, 37 °C for 2 h, 85 °C for 5 min, and the sample was taken out after cooling to 4 °C.

Library preparation was completed through a series of procedures including end-repair, A-tailing, sequencing-adapter ligation, purification, PCR amplification, denaturation and circularization. After library construction, the library was firstly quantified preliminarily by the Qubit fluorometer, and then an Fragment Analyzer was used to detect the insert fragment size so as to guarantee library quality. The quality of the constructed library must pass inspection before sequencing. The detection procedures were described as follows: preliminary quantification was performed by the Qubit fluorometric assay; the insert size of the library was measured with a Fragment Analyzer, and the subsequent experiment could be carried out only when the insert size met the expected standard.

After the library was verified to be qualified, DNA Nano-Balls (DNBs) were prepared and loaded onto the sequencing chip, followed by high-throughput sequencing on a high-throughput sequencer.

The obtained data are converted into fpkm values using the following formula: fpkm = mapped fragments of transcript / Total Count of mapped fragments (Millions) × Length of transcript (kb). Use $P<0.05$ as the criterion to identify differentially expressed genes between groups.

2.9. Determination of neurotransmitter content

Sample pretreatment: Approximately 50 mg of each sample was weighed into a 2-mL centrifuge tube, and the exact weight of each sample was recorded. Immediately, 500 μL of pre-cooled 70 % aqueous methanol extraction solution (−20 °C) was added to the weighed sample, followed by vortexing for 3 min. The mixture was centrifuged at 12 000 r/min for 10 min at 4 °C, and 300 μL of the supernatant was transferred into a 1.5-mL centrifuge tube. The supernatant was kept at −20 °C for 30 min and then centrifuged again at 12 000 r/min for 10 min at 4 °C. Finally, 200 μL of the supernatant was transferred into a sample vial and stored at −20 °C.

Chromatographic-mass spectrometric acquisition conditions: The data-acquisition system consisted of an Ultra-Performance Liquid Chromatography (UPLC) system (ExionLC™ AD) coupled with a Tandem Mass Spectrometry (MS/MS) instrument (QTRAP® 6500+). Chromatographic separation was carried out on an ACQUITY UPLC HSS PFP Column (1.8 μm, 100 mm × 2.1 mm i.d.). Mobile phase A was ultrapure water containing 0.1 % formic acid, and mobile phase B was acetonitrile containing 0.1 % formic acid. The flow rate was set at 0.35 mL/min, column temperature at 40 °C, and injection volume at 2 μL. The mobile-phase gradient was programmed as follows: 0 min, A/B = 95:5 (V/V); 7 min, A/B = 5:95 (V/V); 7.5 min, A/B = 5:95 (V/V); 7.6 min, A/B = 5:95 (V/V); 9 min, A/B = 95:5 (V/V).

Mass spectrometric conditions: The electrospray ionization (ESI) source temperature was 550 °C. The ion-spray voltage was set at 5500 V in positive-ion mode and −4500 V in negative-ion mode. The curtain gas (CUR) pressure was 35 psi. In the QTRAP® 6500+ system, each ion pair was scanned and detected using the optimized declustering potential (DP) and collision energy (CE).

Qualitative and quantitative principles: Quantitative analysis was performed using the multiple-reaction-monitoring (MRM) mode of triple-quadrupole mass spectrometry (as shown in the figure below). After obtaining mass-spectrometry data

from different samples, the chromatographic peaks of all target analytes were integrated, and quantitative analysis was conducted based on the corresponding standard curves.

2.10. Molecular docking verification

Molecular docking between the newly-generated compounds from PR-SSS and key metabolic enzymes involved in tryptophan metabolism was performed using AutoDock software and the Vina program. The target enzymes included indoleamine 2,3-dioxygenase 1 (IDO1), tryptophan 2,3-dioxygenase (TDO), tryptophan hydroxylase 1 (TPH1), kynurenine aminotransferase 1 (KAT1), kynurenine 3-monooxygenase (KMO), aromatic-L-amino-acid decarboxylase (AADC)/dopa decarboxylase (DDC), aralkylamine N-acetyltransferase (AANAT), acetylserotonin O-methyltransferase (ASMT), and monoamine oxidase A (MAO-A). The binding energies and docking images for each protein-ligand complex were obtained, followed by analysis of the docking results. The PDB IDs of docking-targeted proteins and the names of selected ligands are listed in Table 3.

Table 3. The PDB IDs and ligands of docking-targeted proteins

Protein	IDO1	TDO	TPH1	KAT	KMO	AADC	AANAT	ASMT	MAO-A
Crystal structure (PDB)	5EK4	6A4I	8CJM	4GE4	5X68	8ORA	1IB1	4A6D	2BXR
Ligand	5PF	9R9	UXL	0KE	FAD	W5I	COT	SAM	FAD

2.11. Statistical analyses

All experimental results followed a normal distribution. Data were expressed as mean ± standard error of the mean (SEM). One-way analysis of variance (ANOVA) was performed using SPSS 20.0 statistical software. All analyses were completed with GraphPad Prism 9.0 software. For significance testing, differences were considered statistically significant when $P < 0.05$.

3. Results

3.1. Component analysis of SSS and PR-SSS

SSS and PR-SSS herb slices were prepared according to the methods described above. The shape and specifications of the prepared slices are shown in Figure 1 (A) and Figure 1 (B). The two batches of slices were decocted and extracted with water to obtain their corresponding aqueous extracts, which were used for component analysis and subsequent pharmacological experiments. The aqueous extracts of SSS, PR-SSS and PR were analyzed by high-performance liquid chromatography-tandem mass spectrometry (HPLC-MS/MS) to investigate their compositional differences. The results are presented below. The mass-chromatograms of SSS, PR-SSS and PR under ESI^+ and ESI^- are shown in Figure 1 (C–H). Relative quantitative analysis of brucine and strychnine contents in SSS and PR-SSS was performed, and the results are displayed in Figure 1 (I). As illustrated in the figure, the contents of strychnine and brucine in SSS decreased after processing with PR. Specifically, the content of strychnine decreased by 36.23 %, and brucine decreased by 35.62 %. A Venn diagram was applied to analyze the chemical components detected in the aqueous extracts from the three groups of slices, and the transformation and variation rules of components after processing were summarized. The relevant results are shown in Figure 1 (J). There were 26 common components shared by the SSS group and PR-SSS group, among which 10 components were also detected in PR (i.e., common components of all three samples), and the remaining 16 components were original constituents from SSS retained after PR-mediated processing. In PR-SSS, 26 components originated from SSS. Among the other 77 components, 64 were prototype components derived from PR, and 13 were newly-generated compounds, which were presumed to be transformed from the disappeared components of SSS or produced via chemical reactions between constituents from PR and SSS. In addition, 49 components originally present in PR were not detected in PR-SSS. Detailed component detection results are listed in attached list (Table S1-S3).



(**a**)



(**b**)

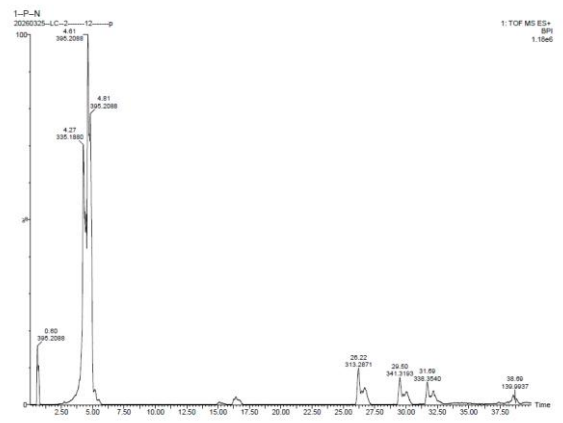

(**c**)

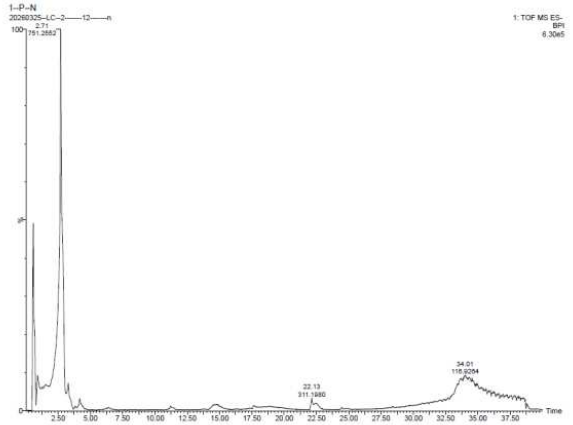

(**d**)

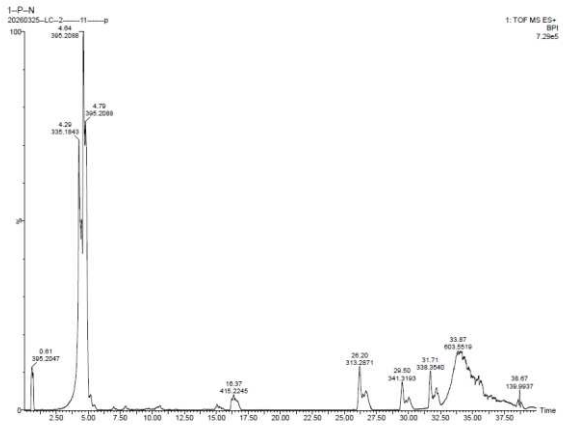

(**e**)

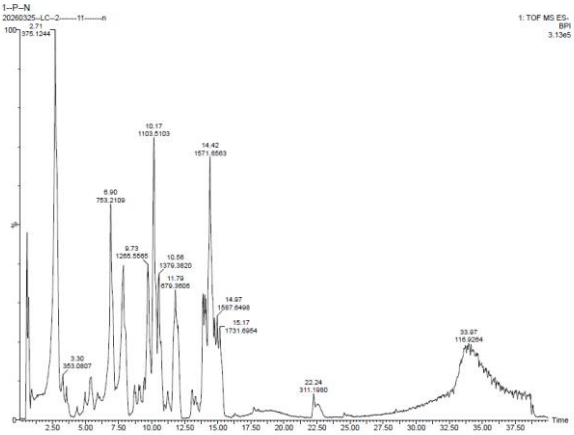

(**f**)

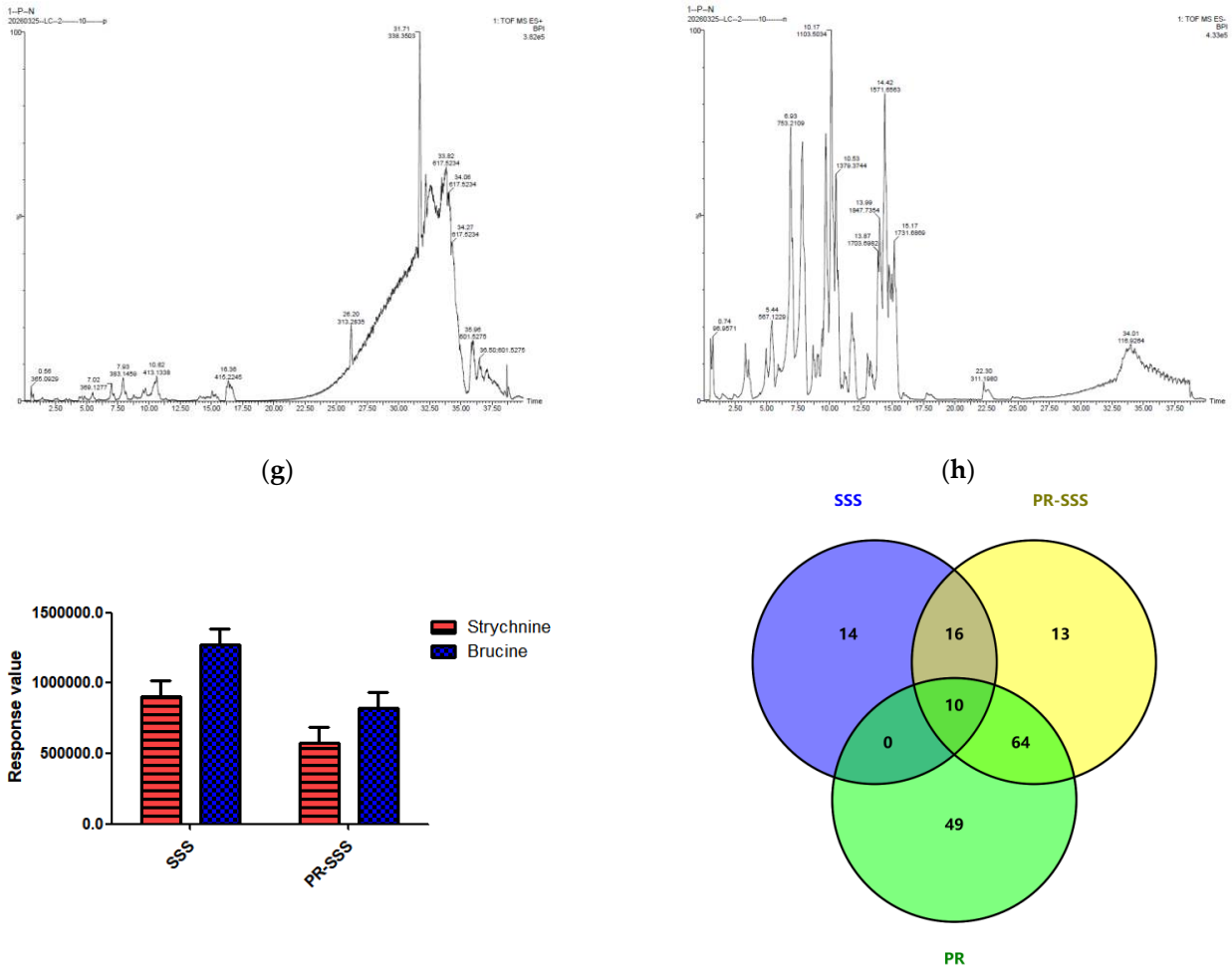

Figure 1. Analysis of the components of SSS and PR-SSS by HPLC-QTOF-MS method. (a, b): The decoction pieces of SSS and PR-SSS. (c-h): Positive and negative ion chromatograms of SSS, PR-SSS and PR. (i): Relative quantification of strychnine and brucine. (j): Venn diagram of the components of SSS, PRSSS, and PR

Considering that 13 new-generated components were produced in the processed product PR-SSS after processing with PR juice (Table 4), it was speculated that the detoxification effect of PR on SSS was closely related to these 13 newly-formed components and the 64 prototype components derived from PR. Therefore, we further investigated and deduced the transformation rules of the 13 newly-generated compounds, and the analytical results are presented as follows. The detailed information of the 13 compounds is listed in the table below (Table 4). Among them, the transformation patterns of Oliveramine, Scroneoside A, Cimicifugamide, Picrasidine C and Compound 11 were elucidated (Figure 2).

Table 4. Newly generated compounds in PR-SSS

No.	Components	Molecular formula	molecular mass/Da	RT/min	Response value	m/z	ppm	Adduct	Ion mode
1	Maltose	$C_{12}H_{22}O_{11}$	342.12	0.60	19503	381.08	3.7	+K, +Na	$[M+H]^+$
2	Guaiacylglycerol 8-O-beta-D-glucopyranoside	$C_{16}H_{24}O_{10}$	376.14	0.62	4542	415.10	1.3	+K	$[M+H]^+$
3	Oliveramine	$C_{20}H_{20}N_2O_4$	352.14	0.61	23204	387.11	8	+Cl	$[M+H]^-$

4	4H-1-Benzopyran-4-one, 2-(3,4-dihydroxyphenyl)-2,3-dihydro-3,7-dihydroxy-5-methoxy-, (2R-cis)- (9CI)	$C_{16}H_{14}O_7$	318.07	0.61	14658	377.09	-4.3	$+CH_3COO$	$[M+H]^-$
5	Scroneoside A	$C_{25}H_{28}O_{11}$	504.16	0.61	5352	539.13	-3.8	+Cl	$[M+H]^-$
6	Oleracein D	$C_{31}H_{37}NO_{17}$	695.21	0.62	4283	695.20	-5.3	+e	$[M+H]^-$
7	Cimicifugamide	$C_{25}H_{31}NO_{10}$	505.19	0.62	12017	540.17	6.7	+Cl	$[M+H]^-$
8	Picrasidine C	$C_{29}H_{26}N_4O_4$	494.20	0.63	6067	539.20	7.3	+HCOO	$[M+H]^-$
9	Inosine	$C_{10}H_{12}N_4O_5$	268.08	0.64	3283	327.09	-3.5	$+CH_3COO$, -H	$[M+H]^-$
10	Parishin D	$C_{20}H_{20}O_9$	404.11	0.70	20495	439.08	-7.5	+Cl	$[M+H]^-$
11	(3,4,5-trihydroxy-6-(1,3,7-trihydroxy-9-oxo-9H-xanthen-2-yl)tetrahydro-2H-pyran-2-yl)methyl (E)-3-(3,4-dimethylphenyl)acrylate	$C_{30}H_{28}O_{11}$	564.16	3.35	7822	563.16	9.7	-H	$[M+H]^-$
12	15α-Hydroxy-cimicifugoside H2	$C_{35}H_{54}O_{11}$	650.37	13.61	8760	649.36	-2.2	-H	$[M+H]^-$
13	3-O-Decanoyl-16-O-acetyl-isoiridogermanal	$C_{42}H_{70}O_6$	670.52	29.60	11723	715.51	-8.5	+HCOO	$[M+H]^-$

397

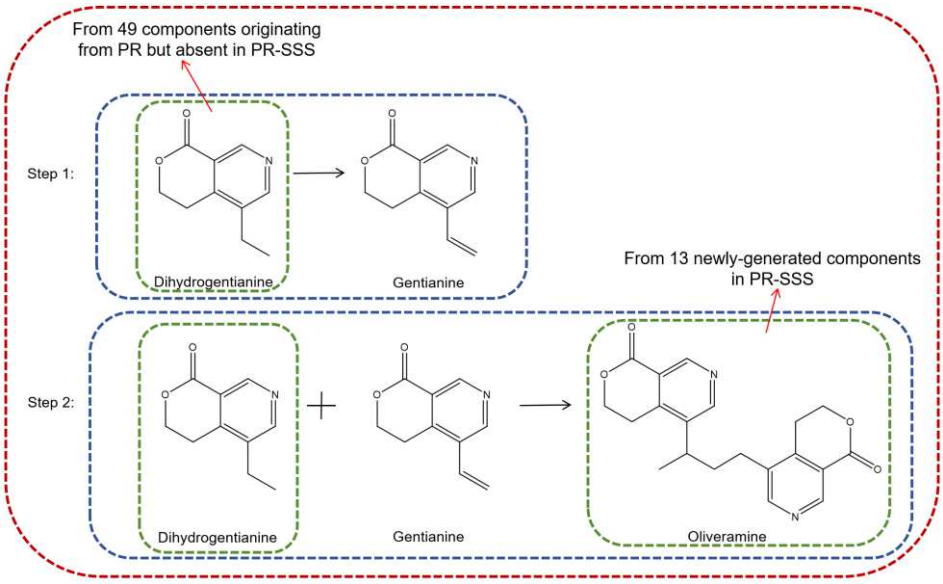

(**a**)

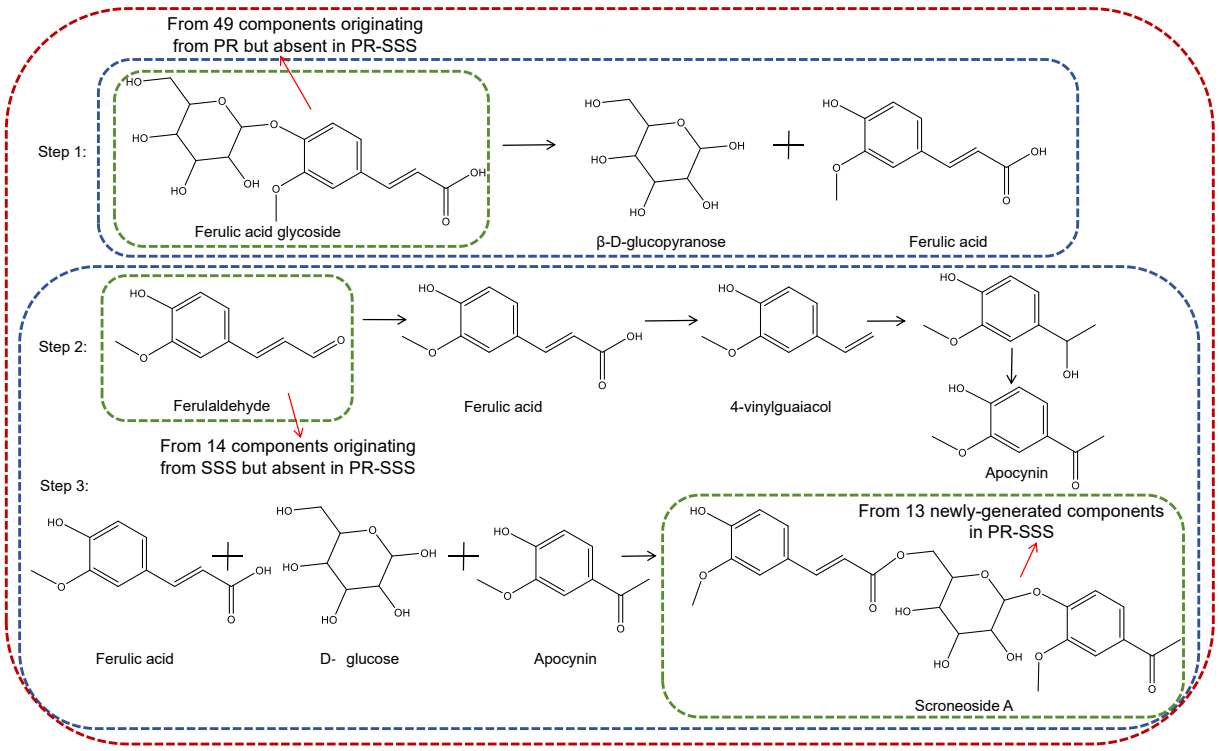
From 49 components originating from PR but absent in PR-SSS
Step 1:
Ferulic acid glycoside
β-D-glucopyranose
Ferulic acid
Step 2:
Ferulaldehyde
Ferulic acid
4-vinylguaiacol
Apocynin
From 14 components originating from SSS but absent in PR-SSS
Step 3:
Ferulic acid
D- glucose
Apocynin
From 13 newly-generated components in PR-SSS
Scroneoside A

(**b**)

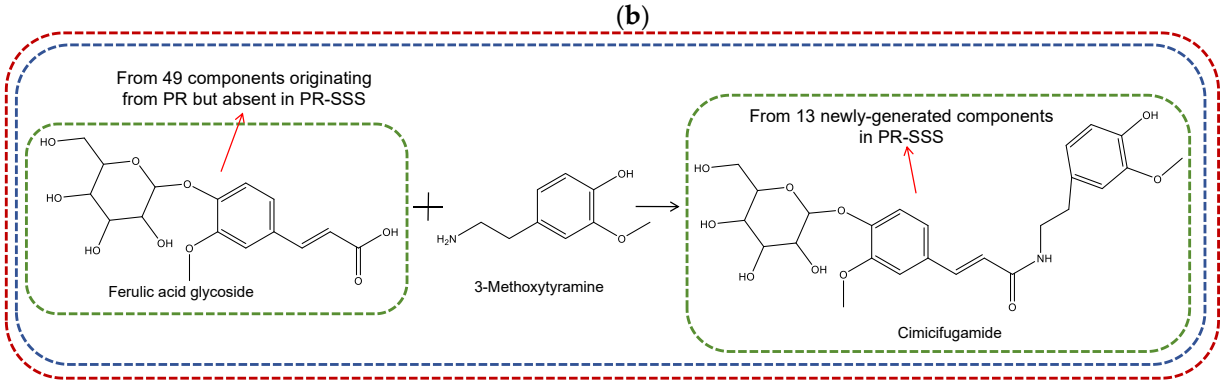
From 49 components originating from PR but absent in PR-SSS
Ferulic acid glycoside
3-Methoxytyramine
From 13 newly-generated components in PR-SSS
Cimicifugamide

(**c**)

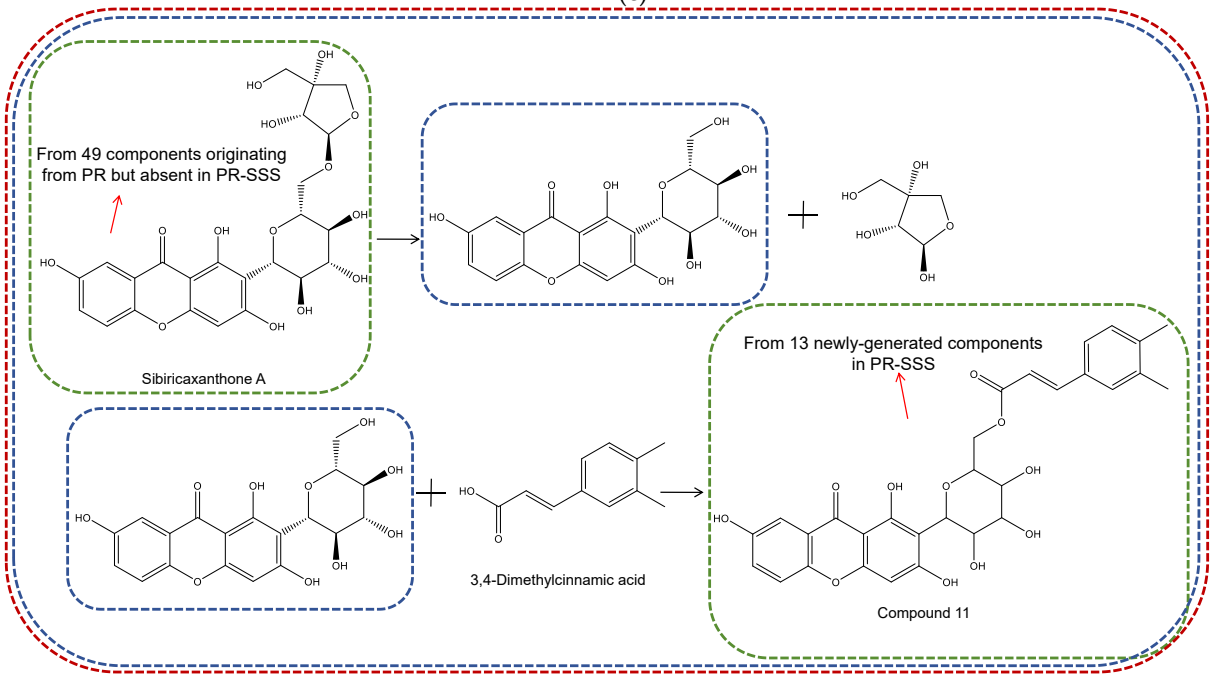
From 49 components originating from PR but absent in PR-SSS
Sibiricaxanthone A
From 13 newly-generated components in PR-SSS
3,4-Dimethylcinnamic acid
Compound 11

(**d**)

Figure 2. Synthetic routes for compounds with favorable molecular docking activity among those newly generated in PR-SSS. (a): Synthetic routes for Oliveramine. (b): Synthetic routes for Scroneoside A. (c): Synthetic routes for Cimicifugamide. (d): Synthetic routes for Compound 11.

3.2. Differences in Acute Toxicity between SSS and PR-SSS

The grouping and experimental results of the acute toxicity test on mice are presented in Table 5. The table reveals that when mice were administered with the decoction of SSS alone, the LD_{50} value was approximately 534.69 mg/kg, indicating significant toxicity. However, when mice were administered with the decoction of PR-SSS, the LD_{50} value increased to 761.46 mg/kg, representing a 42.24% increase in the LD_{50} value of PR-SSS compared to SSS. This suggests that PR-SSS, obtained by decocting PR and SSS together at a 2.5-fold ratio, significantly reduces the mortality of experimental mice caused by SSS. The LD_{50} value has significantly increas ed, indicating that PR significantly mitigates the acute toxicity of SSS.

Table 5. Acute toxic effects of SSS and PR-SSS on mice and their LD_{50} values (n=10)

Groups	Doses/（mg/kg）	Number	Death number	Mortality rate/%	LD_{50}	95% confidence interval
SSS	300	10	0	0	534.69	479.64～596.06
	382	10	2	20		
	486	10	2	20		
	618	10	7	70		
	786	10	10	100		
	1000	10	10	100		
PR-SSS	400	10	2	20	761.46	629.50～921.09
	552	10	3	30		
	761	10	4	40		
	1051	10	7	70		
	1450	10	9	90		
	2000	10	10	100		

3.3. Comparison of the anti-inflammatory and analgesic effects of PR-SSS versus SSS

3.3.1. Mice acetic acid writhing test

The analgesic effect was evaluated using the acetic acid writhing test in mice from different groups; the results are presented in Table 6. Except for the Low-dose PR-SSS group, all administration groups significantly reduced the number of writhing episodes in mice (P <0.05). The analgesic effect of the Low-dose PR-SSS was weaker than that of the corresponding SSS dose; however, the analgesic effects of the Middle-and High-dose PR-SSS groups were superior to those of the SSS group, and the number of writhing episodes in mice receiving the high-dose PR-SSS was comparable to that in the positive (Aspirin) group.

Table 6. The effect of SSS treatment on the number of acetic acid-induced writhing episodes in mice before and after processing of PR（$\bar{x} \pm s$，n=7）

Groups	Doses/（mg/kg）	Number of twisting within 15 minutes
Control group	-	16.00±2.69
SSS	25	6.71±1.39*
	50	6.29±2.24*
	75	5.29±1.80*

	25	12.14±2.05#
PR-SSS	50	5.86±1.32*
	75	3.00±1.07*
Aspirin	20	4.71±1.13*

Compared with the control group, *P<0.05; Compared to the SSS group receiving the same dose, #P <0.05.

3.3.2. Mice hot plate assay

The experimental results are presented in Table 7. The results indicate that there were no significant differences in the baseline pain thresholds among the various groups; thus, the data from all groups are considered comparable. At 30, 60, 90 and 120 min post-administration, compared to the control group at the corresponding time points, the pain latency in mice across all groups was significantly prolonged—except for the Low-and Medium-dose SSS group at 30 min—as evidenced by an increased duration of leg-raising time (P <0.05). This suggests that both the raw and processed SSS can elevate the pain threshold in mice and exhibit analgesic effects; furthermore, compared to the SSS group receiving the same dose at the corresponding time points, the PR-SSS group demonstrated a significant prolongation of the leg-raising time in mice receiving the Medium dose at 30 and 60 minutes, as well as the Low dose at 90 and 120 minutes (P <0.05); at all other time points, the analgesic effect was comparable to that observed with the same dose.

Table 7. The effect of SSS before and after processing with PR on the mouse hot-plate test with mice leg-raising time（$\bar{x}\pm s$，$n=7$）

Groups	Doses/（mg/kg）	Basic pain threshold / s	30 min / s	60 min / s	90 min / s	120 min / s
Control group		16.57±1.00	16.83±0.62	16.44±0.34	17.13±0.32	17.26±0.20
SSS	25	17.14±1.97	18.84±0.63	20.61±0.29*	20.26±0.24*	18.61±0.40*
	50	16.14±1.06	17.64±0.86	21.41±0.70*	23.86±0.48*	23.44±0.64*
	75	17.86±1.12	24.63±0.84*	27.00±0.61*	27.54±0.70*	28.09±0.40*
PR-SSS	25	17.10±1.66	19.39±0.70*	21.67±0.49*	21.29±0.24*#	20.44±0.31*#
	50	17.64±1.90	20.80±0.20*#	23.76±0.40*#	24.87±0.23*	23.13±0.81*
	75	18.07±1.49	24.54±0.43*	27.04±0.25*	27.10±0.49*	26.90±0.52*
Aspirin	20	16.79±1.22	28.63±0.58*	29.83±0.79*	30.19±0.31*	30.54±0.39*

At the same time, compared with the control group, *P<0.05; Compared to the SSS group receiving the same dose, #P <0.05.

3.3.3. Mice xylene-induced ear swelling experiment

The results of the ear swelling experiment are presented in Table 8. The experimental data demonstrated that, compared to the control group, all experimental groups, except for the Low-dose SSS group, significantly reduced the degree of xylene-induced ear swelling in mice (P <0.05); furthermore, the swelling degree in the Low-dose PR-SSS group was significantly lower than that in the Low-dose SSS group (P <0.05), indicating that the anti-inflammatory efficacy of PR-SSS is superior to that of SSS.

Table 8. The effect of SSS before and after processing with PR on mouse ear swelling model（$\bar{x}\pm s$，$n=7$）

Groups	Doses/（mg/kg）	Ear swelling degree / mg
Control group	-	4.97±0.71
SSS	25	3.56±0.33
	50	2.77±0.58*
	75	1.50±0.32*
PR-SSS	25	2.26±0.28*#
	50	2.31±0.18*
	75	1.53±0.25*

Aspirin	20	1.30±0.18*

Compared with the control group, *P<0.05; Compared to the SSS group receiving the same dose, #P <0.05.

3.4. Subchronic toxicity in the central nervous system of rats

3.4.1. Results of body weight, balance beam, and open field tests in rats.

Sprague-Dawley (SD) rats were randomly divided into groups and administered with corresponding drugs for 15 consecutive days. Figure 3A shows the body weight of rats in each group after 15-day administration. Compared with the normal group, the body weight of rats in the SSS-H group decreased significantly. At the same dosage, the body weight of the PR-SSS group increased markedly relative to the SSS group and returned to the normal level.Figure 3B presents the time taken by SD rats to cross the balance beam in the balance-beam test on day 14 of administration. The crossing time was significantly prolonged in the SSS-H group. At the high dosage, the PR-SSS group exhibited a remarkably shorter crossing time compared with the SSS group, indicating that the chronic neurotoxicity of PR-SSS was markedly reduced.Figure 3C displays the movement trajectories of rats in the open-field test on day 14. Rats in the normal group showed active locomotor trajectories and centripetal exploratory behaviors within 5 min. In the SSS groups, the range of movement trajectories gradually decreased with the increase of dosage. Rats in the SSS-H group only exhibited wall-hugging activities along two side walls. By contrast, the locomotor activity was significantly enhanced in all PR-SSS groups. Obvious differences in movement trajectories were observed between PR-SSS-H and SSS-H groups, whereas no significant difference was found between the PR group and the normal group.Figure 3D shows the total travel distance in the open-field test. The travel distance was significantly shortened in the SSS-H group. Compared with the SSS-H group at the same dosage, the PR-SSS-H group achieved a markedly longer travel distance with higher locomotor activity. These results suggested that rats treated with SSS suffered from varying degrees of nerve injury, while PR-SSS could alleviate such chronic neurotoxicity.

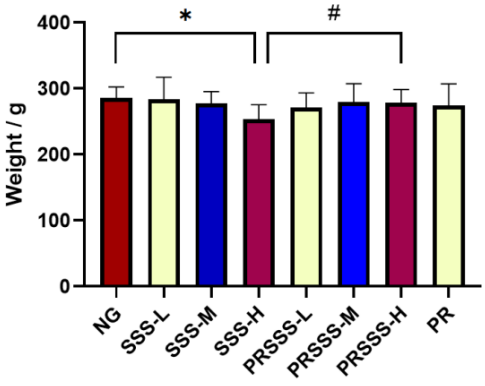

(**a**)

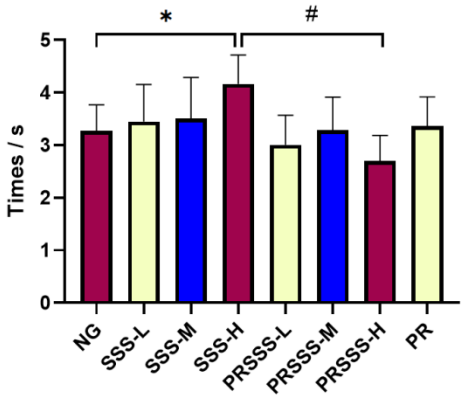

(**b**)

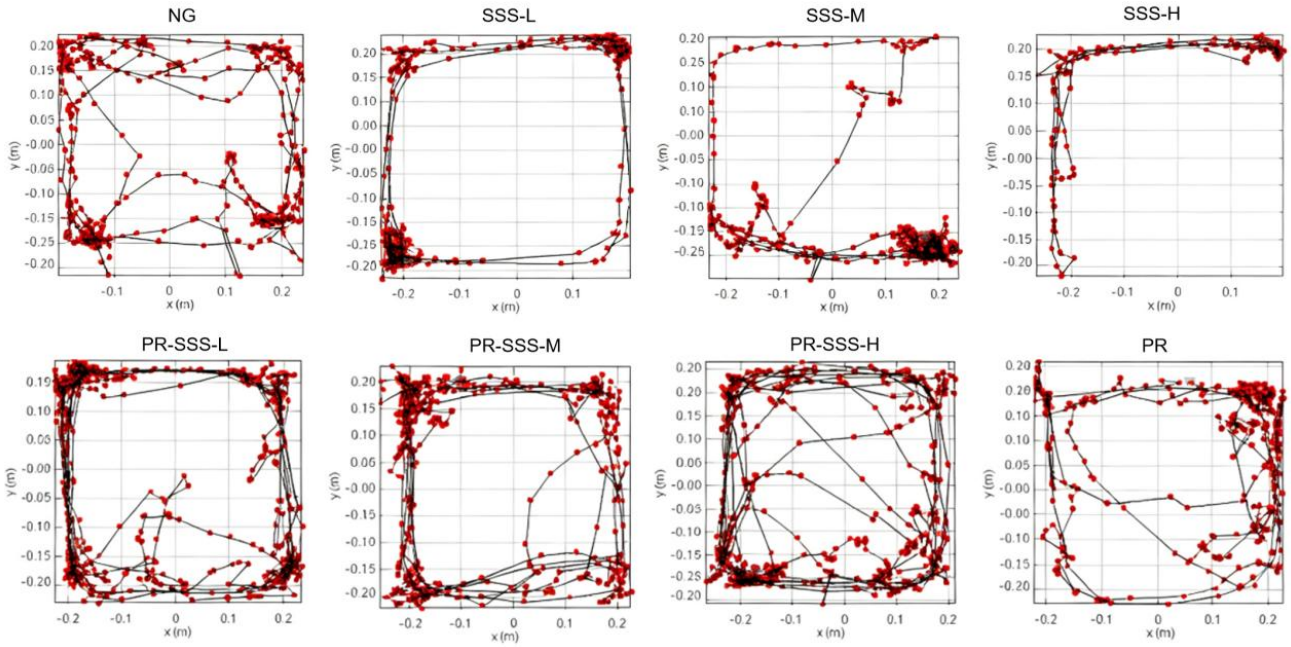

(**c**)

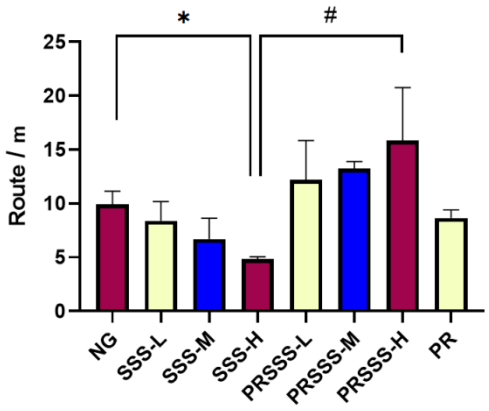

(**d**)

Figure 3. Results of body weight, balance beam, and open field tests in rats. (a): Body weight of rats in each group (15d). (b): The time taken by rats to cross the balance beam (15d). (c): Open field movement trajectory of rats in each group. (d): The open field movement distance of rats in each group. In Figure A,B and D, compared with the NG, $^{*}P<0.05$; compared to the SSS group receiving the same dose, $^{\#}P<0.05$, $n=10$.

3.4.2. Pathological examination of rat brain tissue

The HE staining results of rat brain tissues are shown in Figure 4. In the normal group, the cells in the hippocampus were arranged in an orderly manner. By contrast, the hippocampal nerve cells in the high-dose SSS group exhibited lighter staining and cytoplasmic vacuolation, indicating a certain degree of tissue injury. This pathological change was alleviated in the high-dose PR-SSS group, and the hippocampal neurons in the PR group were nearly normal. Nissl-body staining results revealed abundant Nissl staining in the hippocampus of rats from the normal group and PR group. Fewer Nissl-positive signals together with vacuolation were observed in the high-dose SSS group, whereas PR-SSS treatment ameliorated these pathological manifestations.

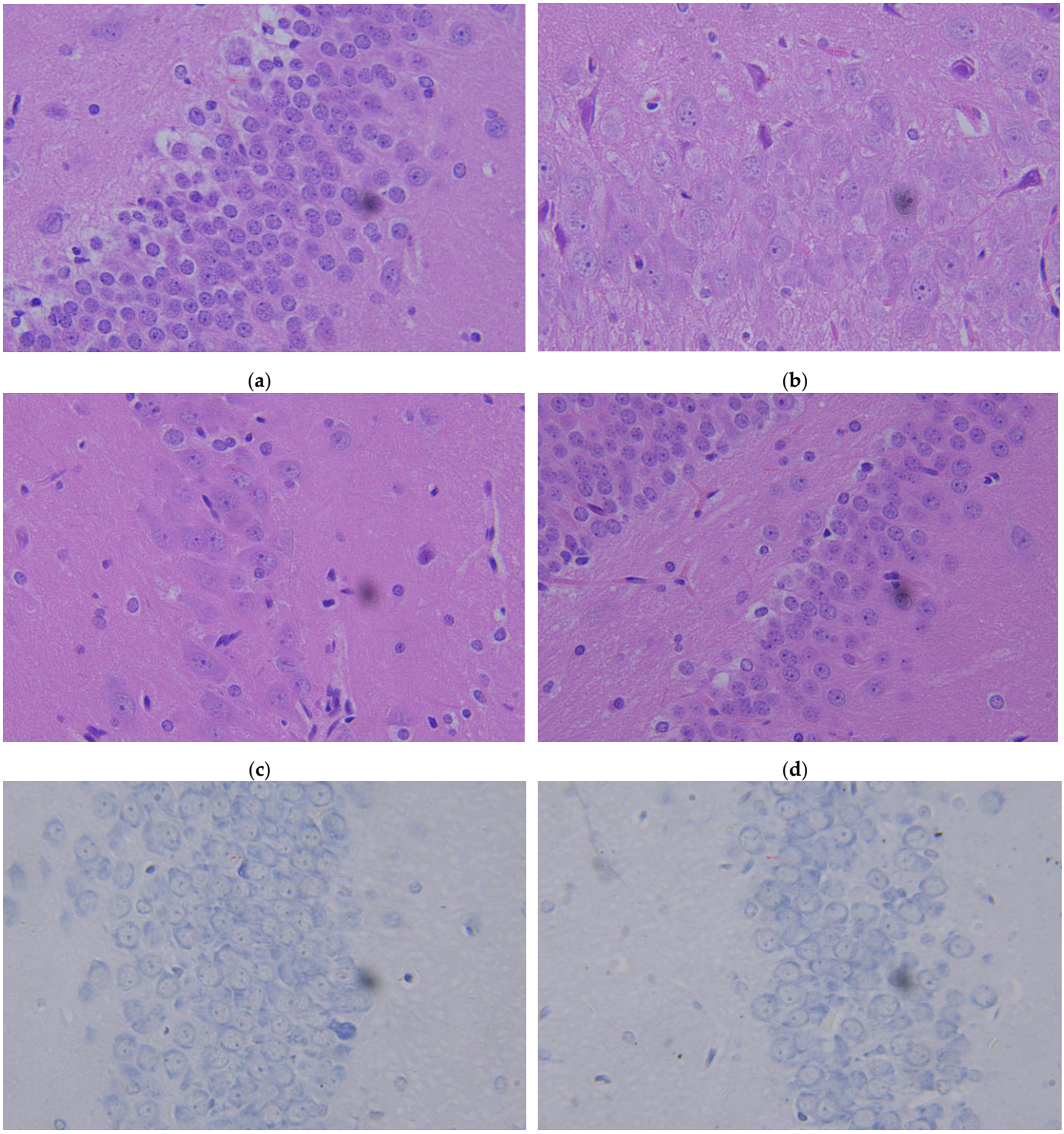

(**a**) (**b**)

(**c**) (**d**)

(**e**) (**f**)

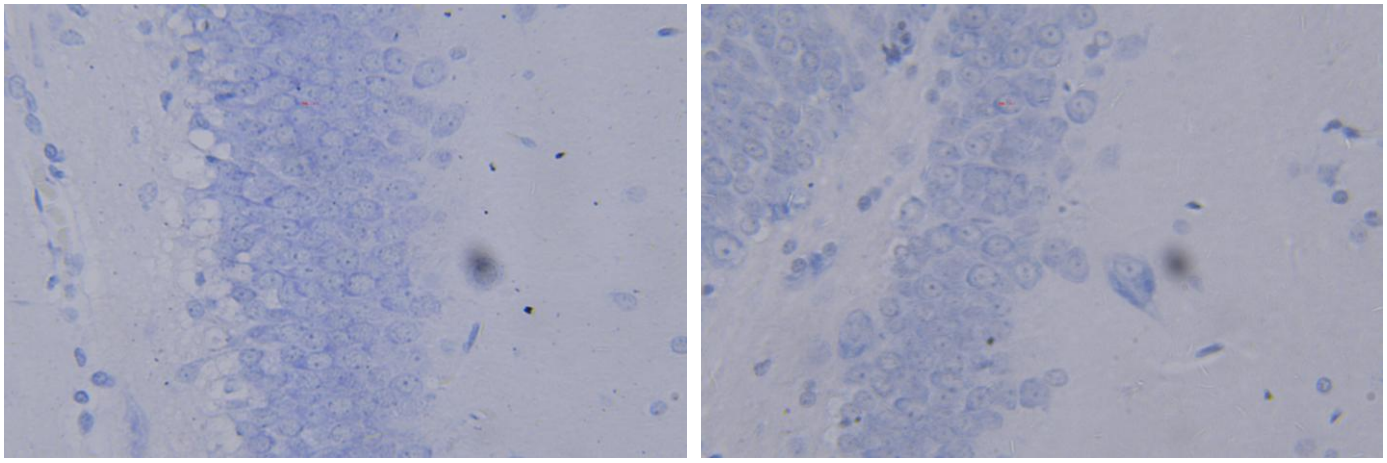

(**g**) (**h**)

Figure 4. Rat brain tissue histopathological staining results. (a): Normal group for HE staining; (b): SSS-H for HE staining; (c): PR-SSS-H for HE staining; (d): PR for HE staining; (e): Normal group for Nissl staining; (f): SSS-H for Nissl staining; (g): PR-SSS-H for Nissl staining; (h): PR for Nissl staining (×400).

3.5. The mechanism by which PR reduces the toxicity of SSS based on cerebral metabolomics

In the sub-chronic toxicity experiment, rats were sacrificed after 15 consecutive days of administration. Brain tissues were collected, homogenized, processed and subjected to metabolomic detection. Since prominent toxic differences were observed in the high-dose groups during the behavioral tests of the sub-chronic toxicity study, samples from the high-dose SSS and PR-SSS groups were selected for metabolomic processing and analysis, and the results are shown in Figure 5.

Brain-tissue samples from the NG, SSS and PR-SSS groups were detected and analyzed. Compound identification and relative-quantitative comparison were performed by matching against databases. Principal component analysis (PCA) and orthogonal partial least-squares discriminant analysis (OPLS-DA) were conducted for all samples. The results indicated that PCA could not achieve satisfactory separation, whereas favorable discrimination was obtained between the SSS and PR-SSS groups in the OPLS-DA model.

Differential metabolites between the two groups were screened with the thresholds of $P < 0.05$ and VIP > 1. The volcano plot of differential metabolites between PR-SSS and SSS is presented in Figure 5C-D. A total of 138 differential metabolites were identified out of 2976 metabolites, including 73 up-regulated and 65 down-regulated compounds. The heatmaps of differential metabolites among SSS and PR-SSS groups are shown in Figure 5E.

KEGG and GO enrichment analyses of the differential metabolites between PR-SSS and SSS were performed (Figure 5F). Metabolite-set enrichment analysis was carried out via the MetaboAnalyst website (https://www.metaboanalyst.ca/). The results revealed that six metabolic pathways showed significant differences ($P < 0.05$), namely nicotinate and nicotinamide metabolism, taurine and hypotaurine metabolism, arginine biosynthesis, alanine, aspartate and glutamate metabolism, glycine, serine and threonine metabolism, and tryptophan metabolism.

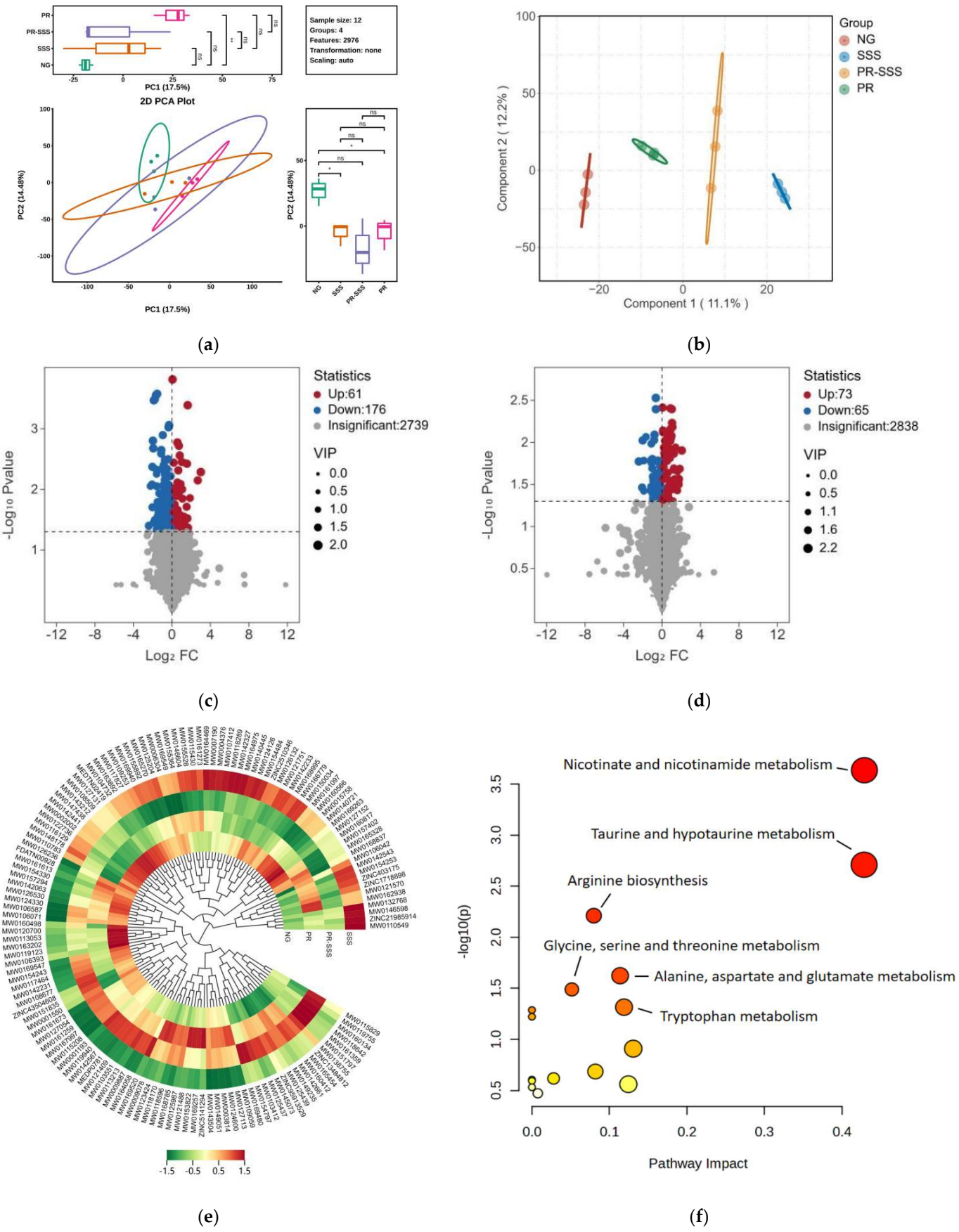

Figure 5. Statistical analysis of cerebral metabolites in the SSS and PR-SSS groups (n = 3 per group). (a): PCA analysis of the overall sample. (b): OPLS-DA analysis of the overall sample. (c, d): Differential metabolite volcano plot of the NG and

SSS, SSS and PR-SSS groups. (e): Differentially abundant metabolite heatmap of the SSS and PR-SSS groups. (f): Enrichment pathway Bubble plot of the SSS and PR-SSS groups.

3.6. Brain tissue transcriptomics detection

A differential analysis was performed on the 14,958 genes identified through database alignment: in the SSS and NG groups, 249 genes were significantly upregulated and 482 genes were significantly downregulated (Figure 6(A)); in the PR-SSS and SSS groups, 682 genes were significantly upregulated and 440 genes were significantly downregulated (Figure 6(B)).

Transcriptomic results of rat brain tissues are presented in Figure 6. Compared with the SSS group, the most significantly enriched pathway of differentially expressed genes in the PR-SSS group was the circadian rhythm pathway, which was highly consistent with the tryptophan metabolism pathway enriched by differential metabolites in the previous brain-tissue metabolomic analysis. Melatonin, an important regulator of circadian rhythm, is a key product of the serotonin-melatonin metabolic branch within tryptophan metabolism. In addition, transcriptomic enrichment results indicated that the differentially expressed genes were enriched in pathways such as ubiquitin-mediated proteolysis and protein processing in the endoplasmic reticulum. Therefore, we hypothesized that PR could affect the synthesis and ubiquitination-dependent degradation of various metabolic enzymes involved in the tryptophan-kynurenine-kynurenic acid and tryptophan-serotonin-melatonin pathways, and further modulate neurotransmitter metabolism in the brain tissues of rats in the PR-SSS and SSS groups.

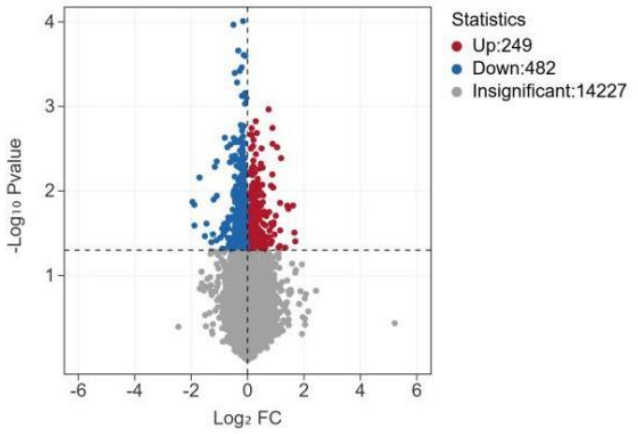

(**a**)

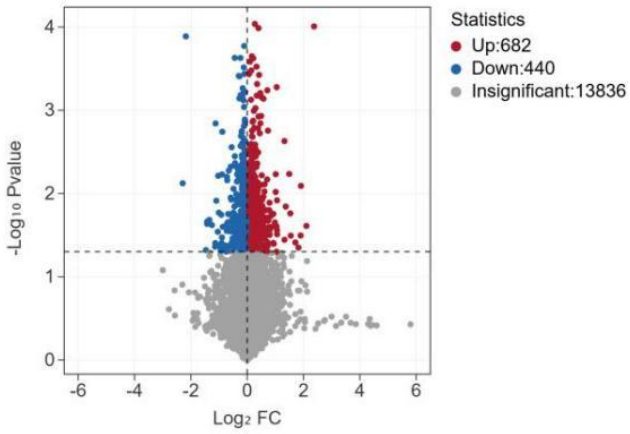

(**b**)

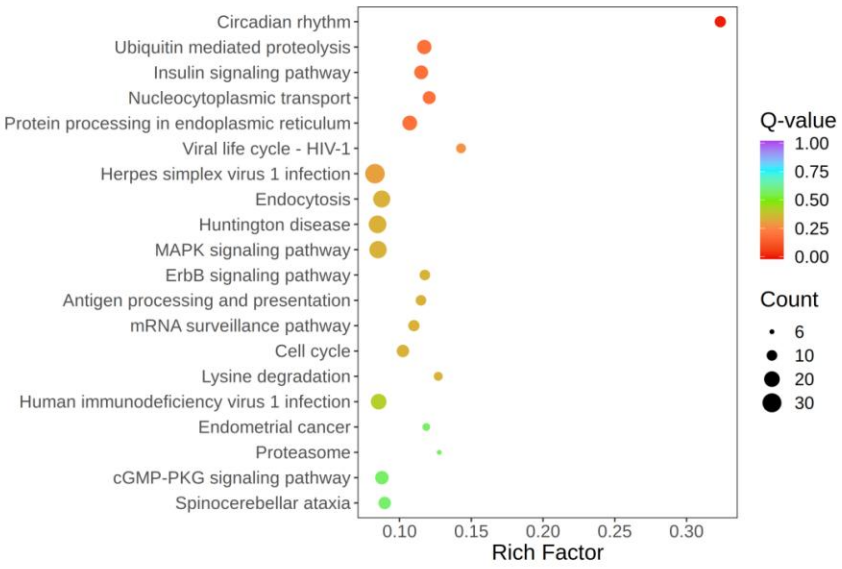

(**c**)

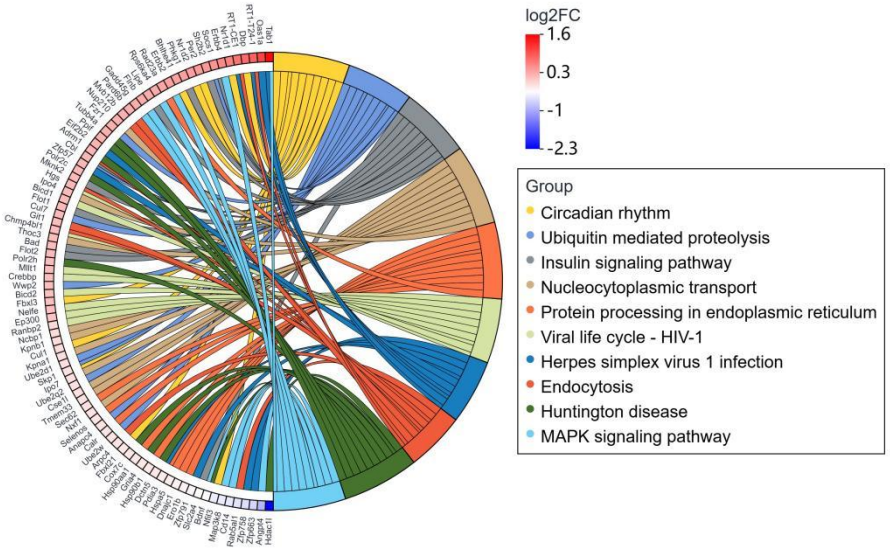

(**d**)

Figure 6. Statistical analysis of cerebral genes in the SSS and PR-SSS groups (n = 3 per group). (a, b): Differential genes volcano plot of the NG and SSS, SSS and PR-SSS groups. (c): KEGG pathway enrichment heatmap showing differentially expressed genes between the PR-SSS and SSS groups. (d): PR-SSS vs. SSS group differential gene enrichment pathway and chord diagram.

3.7. Detection of neurotransmitters with tryptophan metabolic pathway in brain tissue

The mechanistic diagram of the tryptophan metabolic pathway is shown in the figure. Tryptophan metabolism is divided into three major pathways: 1. the kynurenine metabolic pathway, which accounts for 95 % of tryptophan metabolism and is responsible for the metabolism of the vast majority of tryptophan; 2. the serotonin biosynthetic pathway, which accounts for approximately 5 % and serves as the synthetic pathway for brain-derived serotonin; serotonin can be catabolized into inactive products by monoamine oxidase (MAO) and excreted via urine, and can also be converted into N-acetyl-5-hydroxytryptamine under the catalysis of N-acetyltransferase for further biosynthesis of melatonin, a critical hormone regulating circadian rhythm; 3. the indole metabolic pathway, which accounts for a very small proportion and is mainly mediated by intestinal microbiota in the gut.

In the present study, liquid chromatography-mass spectrometry was further adopted to determine the contents of key neurotransmitters in rat brain tissues after administration of SSS before and after PR processing. As shown in the figure below, the proportion of metabolites flowing into the kynurenine-kynurenic acid branch was significantly up-regulated in the tryptophan metabolic pathway of the SSS group, while this proportion was markedly down-regulated in the PR-SSS group compared with the SSS group, indicating that the kynurenine metabolic branch of tryptophan metabolism was inhibited in PR-SSS-treated rats. In the serotonin biosynthetic pathway, the relative levels of serotonin, 5-hydroxyindole-3-acetic acid and N-acetyl-5-hydroxytryptamine were significantly increased in the PR-SSS group relative to the SSS group. Combined with the enrichment results of differential metabolites and differentially expressed genes obtained from brain-tissue metabolomics and transcriptomics, these findings demonstrated that PR intervention shifted the metabolic flux of tryptophan in SSS from the kynurenine-predominant pathway toward the serotonin-melatonin biosynthetic pathway, which might represent the principal mechanism by which PR attenuates the neurotoxicity induced by SSS (Figure 7).

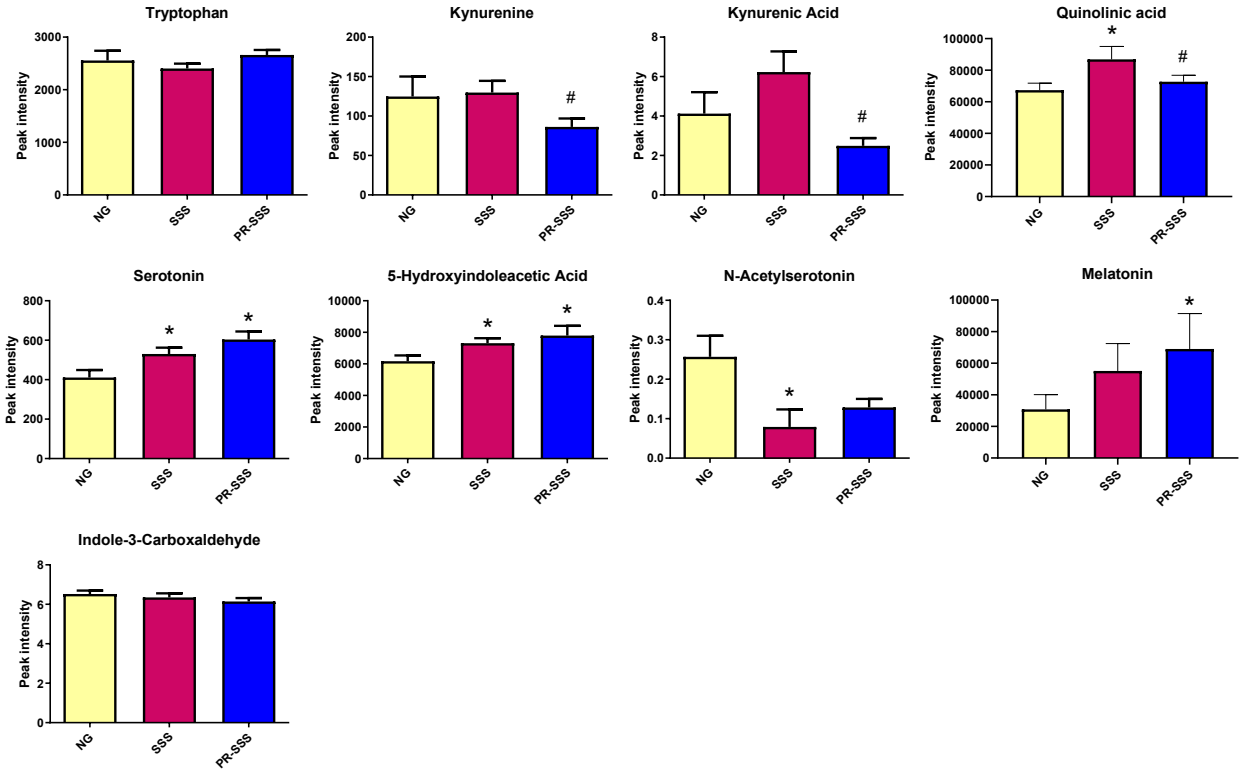

Figure 7. Relative quantification of cerebral Neurotransmitters of Tryptophan metabolic pathway in the SSS and PR-SSS groups (n = 6 per group). In Figure, compared with the NG, $^{*}P<0.05$; compared to the SSS group, $^{\#}P<0.05$.

3.8. Molecular Docking between Newly-Generated Compounds and Key Target Proteins of the Tryptophan Pathway

Molecular docking was performed between the 13 newly-formed components in the PR-SSS group, including Oliveramine, Scroneoside A, Cimicifugamide, Picrasidine C and Compound 11, and the enzymes responsible for synthesis and ubiquitination-dependent degradation involved in the rate-limiting enzymatic reactions of the tryptophan-kynurenine metabolic pathway and the tryptophan-serotonin-melatonin metabolic pathway. The results are shown in Figure 8.

Among the proteins downloaded from the PDB website (https://www.rcsb.org/), the key enzymes in the kynurenine metabolic pathway—IDO1, TDO, KAT, and KMO—adopt an inhibitory conformation; the lower their binding energy to a compound, the more stable the binding, and upon compound binding, these enzymes tend to stabilize the inhibitory protein conformation (represented by blue squares, with darker shades indicating lower binding energy). In contrast, the key enzymes in the 5-HT biosynthetic pathway—TPH1, AADC, AANAT, and ASMT—adopt an activating conformation; likewise, the lower their binding energy to a compound, the more stable the binding, and upon compound binding, these enzymes tend to stabilize the activating protein conformation (represented by red squares, with darker shades indicating lower binding energy).

Molecular docking results indicate that Oliveramine exhibits favorable molecular docking energies when complexed with IDO1, TPH1, KAT, AADC, AANAT, and ASMT; Scroneoside A shows favorable docking energies when complexed with IDO1, TDO, TPH1, KAT, KMO, and AANAT; Cimicifugamide demonstrates favorable molecular docking energies when complexed with TPH1, KAT, KMO, AADC, AANAT, and ASMT; and Compound 11 exhibits favorable molecular docking energies when complexed with IDO1, TDO, TPH1, KAT, KMO, and AANAT, all of these docking energies are < − 7 kcal/mol. All of them form hydrogen bonds.

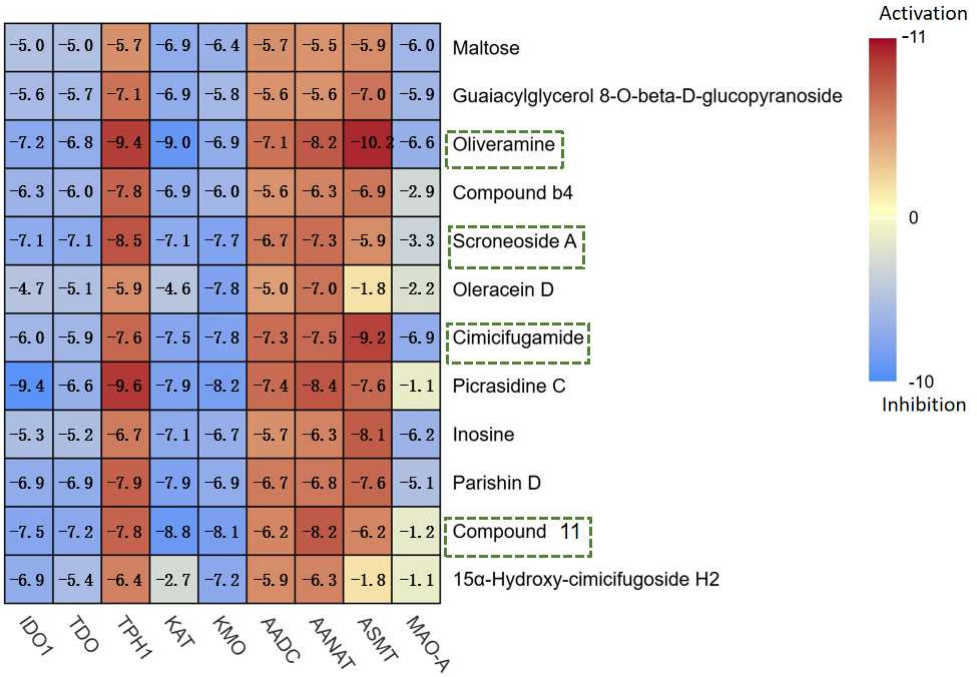

(**a**)

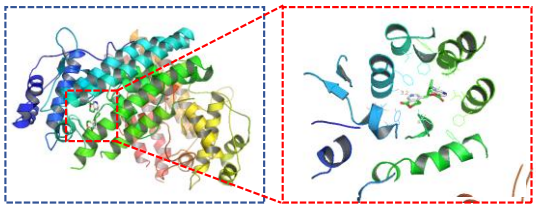

Oliveramine and IDO1

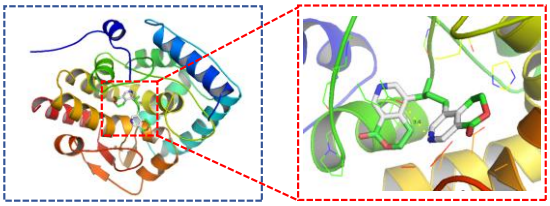

Oliveramine and TPH1

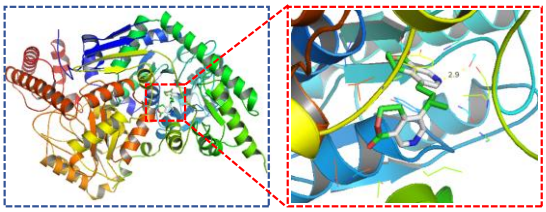

Oliveramine and KAT

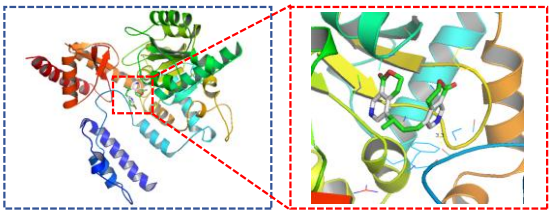

Oliveramine and AADC

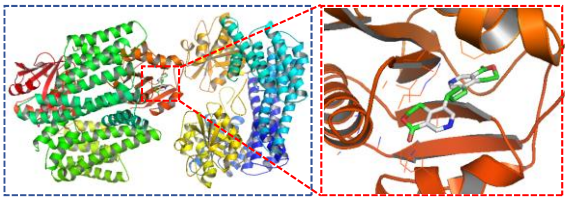

Oliveramine and AANAT

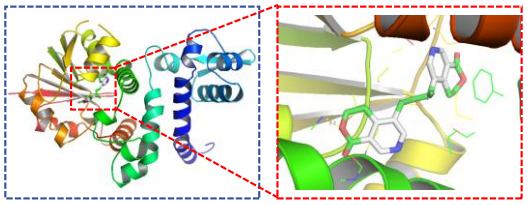

Oliveramine and ASMT

(**b**)

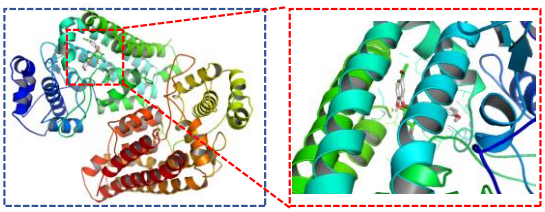

Scroneoside A and IDO1

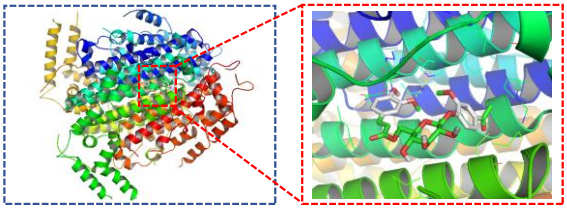

Scroneoside A and TDO

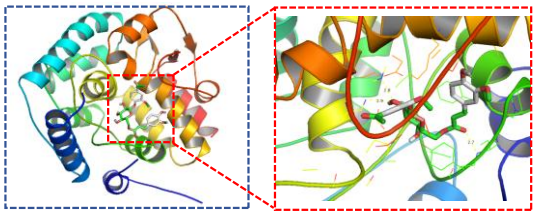

Scroneoside A and TPH1

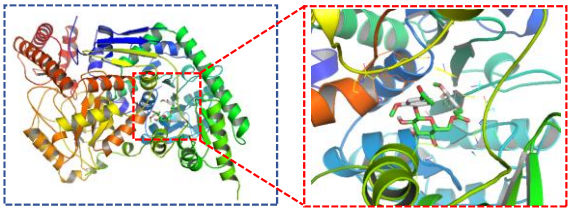

Scroneoside A and KAT

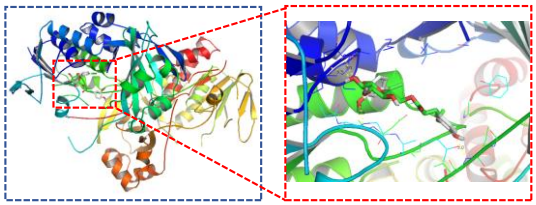

Scroneoside A and KMO

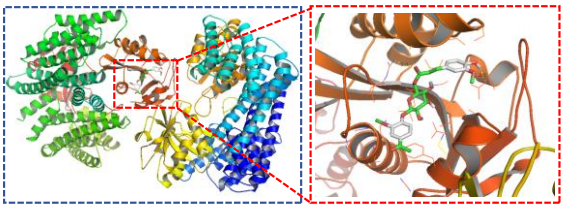

Scroneoside A and AANAT

(**c**)

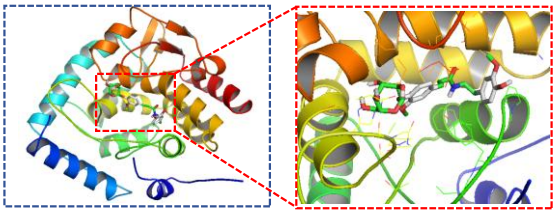

Cimicifugamide and TPH1

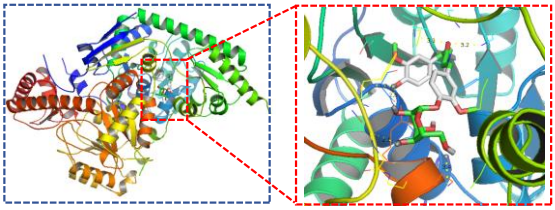

Cimicifugamide and KAT

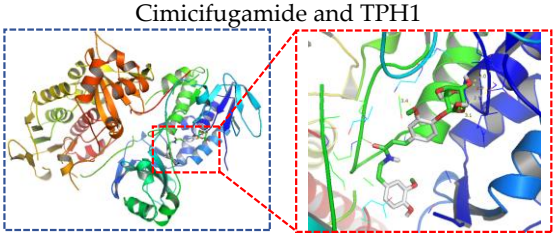

Cimicifugamide and KMO

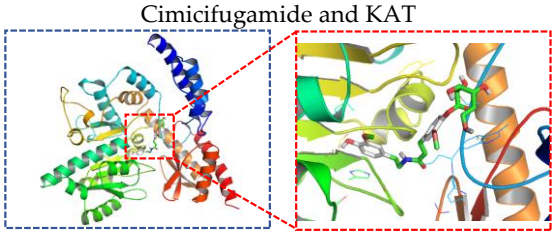

Cimicifugamide and AADC

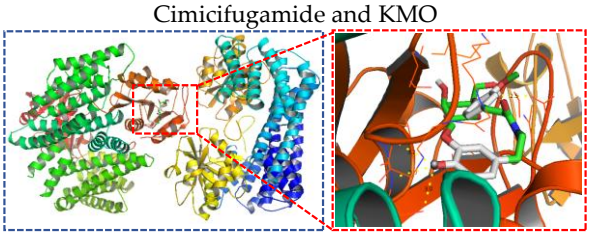

Cimicifugamide and AANAT

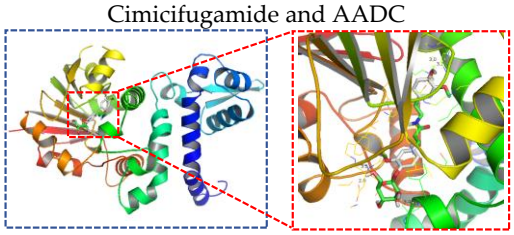

Cimicifugamide and ASMT

(**d**)

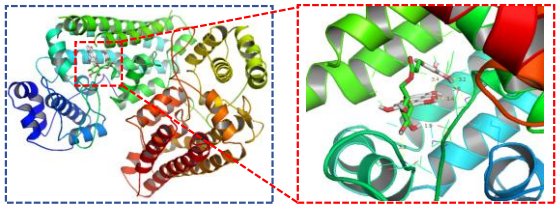

Compound 11 and IDO1

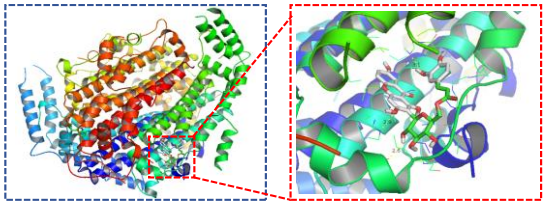

Compound 11 and TDO

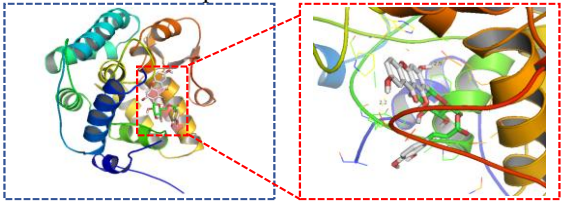

Compound 11 and TPH1

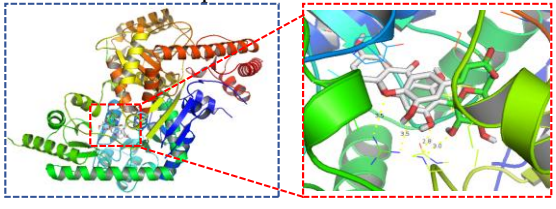

Compound 11 and KAT

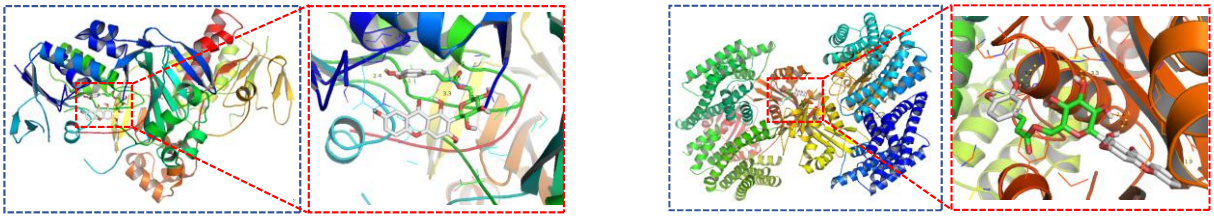

Compound 11 and KMO　　Compound 11 and AANAT

(**e**)

Figure 8. Molecular docking results for newly generated compounds against key target proteins in the tryptophan pathway. Red indicates activation, while blue indicates inhibition; the darker the color, the lower the binding energy. (a): Molecular docking energy of newly generated compounds against key target proteins in the tryptophan metabolic pathway (kcal/mol). (b): Molecular docking of Oliveramine with key target proteins. (c): Molecular docking of Scroneoside A with key target proteins. (d): Molecular docking of Cimicifugamide with key target proteins. (e): Molecular docking of Compound 11 with key target proteins.

4. Discussion

The overlap between toxic and active constituents is an important reason for the narrow safety range of SSS. SSS is rich in alkaloids, which account for 1.5–5.0 % of the medicinal material. Strychnine and brucine make up 80 % of the total alkaloids, among which strychnine accounts for 40–50 % and brucine accounts for 30–40 %; both compounds are the major toxic and bioactive components of nux-vomica [3]. The overlap of toxic-effective constituents constitutes the primary cause for its narrow therapeutic window and limited clinical application. Strychnine and brucine in nux-vomica exert different toxic effects, mainly manifested as central neurotoxicity. Strychnine can inhibit the degradation of acetylcholine (ACh) by acetylcholinesterase (AChE), resulting in the accumulation of ACh in the synaptic interstitium and further triggering cholinergic nerve excitation [7]. Other studies have reported that strychnine blocks glycine receptors (glycine is an inhibitory neurotransmitter), leading to abnormal neuronal excitation and epileptiform-like symptoms[8, 9]. Brucine also exhibits neurotoxicity, although its toxicity is slightly weaker than that of strychnine; it can block neuromuscular conduction and produce curare-like effects by competing with acetylcholine for nicotinic acetylcholine receptors (nAChRs) on the postsynaptic membrane at the neuromuscular junction. After binding to these receptors, brucine prevents the normal opening of sodium ion channels and suppresses postsynaptic potential changes, thereby blocking the transmission of nerve impulses at the neuromuscular junction, which may cause respiratory muscle paralysis and suffocation-induced death in severe cases. Nevertheless, brucine is well-known for its anti-inflammatory and analgesic activities [7]. Taken together, these references indicate that SSS poisoning is mainly characterized by abnormal excitation of the central nervous system. In the present study, after processing with PR, the contents of the toxic components strychnine and brucine in SSS decreased by 36.23 % and 35.62 %, respectively. These findings suggest that PR-mediated processing reduces the levels of toxic constituents in SSS while its anti-inflammatory and analgesic effects are well-preserved, even showed a significant increase compared to the same dose.

PR-SSS obtained after processing with PR could significantly reduce the acute toxicity of SSS and increase the LD_{50} value in acutely-poisoned mice ($P < 0.05$). It also remarkably improved behavioral performance in rats with sub-acute toxicity, including markedly shortening the traversal time on the balance-beam test ($P < 0.05$) and significantly increasing the total travel distance in the open-field test ($P < 0.05$) of SSS-poisoned rats, as well as obviously ameliorating the histopathological injury in the hippocampus of SSS-poisoned rats. These results indicated that PR-SSS could alleviate the central-nervous-system toxicity induced by SSS in both short-term and sub-chronic exposure, which verified the medication experience of folk practitioners in Guizhou and confirmed the detoxification effect of SSS processed with PR.

To explore the detoxification mechanism after PR-mediated processing, metabolomics combined with transcriptomics was applied in this study. Compared with unprocessed SSS, the differential metabolites of PR-SSS were significantly enriched in six metabolic pathways including nicotinate and nicotinamide metabolism, taurine and hypotaurine metabolism, arginine

biosynthesis, alanine, aspartate and glutamate metabolism, glycine, serine and threonine metabolism and tryptophan metabolism ($P < 0.05$). Transcriptomic results revealed significant enrichment in the circadian rhythm pathway, as well as pathways such as ubiquitin-mediated proteolysis and protein processing in the endoplasmic reticulum. The circadian rhythm pathway acts as a downstream pathway of tryptophan metabolism and is closely associated with tryptophan metabolism [10]. Therefore, the tryptophan metabolic pathway was identified as the common pathway enriched by both metabolomic and transcriptomic data. It can be concluded that PR-SSS exerts its detoxification effect mainly through regulating the tryptophan metabolic pathway, and this effect is closely related to the ubiquitin-dependent degradation, endoplasmic-reticulum-associated synthesis and activity of key enzymes within this pathway.

Tryptophan metabolism is closely related to various neurological disorders such as cognitive dysfunction, depression and Alzheimer's disease [11]. Its metabolic pathways mainly include the kynurenine pathway (85 %), the serotonin pathway (5 %) and the intestinal indole metabolic pathway (10 %) [12]. Most metabolites in the kynurenine pathway, such as kynurenine and quinolinic acid, are inducers of neuronal inflammation [13]. As vital neurotoxic substances, they exert pro-oxidant, pro-inflammatory, pro-apoptotic and glutamate-receptor-activating effects. Meanwhile, these metabolites can be induced by inflammatory cytokines including TNF-α and IL-6, which interact reciprocally and trigger a vicious cycle of neuronal injury [14]. The enrichment results of brain-tissue metabolomics and neurotransmitter detection of the tryptophan pathway demonstrated that metabolites of the kynurenine pathway were significantly up-regulated in the SSS group, which was consistent with the behavioral and hippocampal histopathological findings. By contrast, the kynurenine pathway was markedly down-regulated while the serotonin pathway was significantly enhanced in the PR-SSS group compared with the SSS group. Modern pharmacological studies have confirmed that serotonin-related metabolites derived from tryptophan such as 5-HT possess neuroprotective and antidepressant properties. This metabolic alteration in the PR-SSS group explained the remarkable increase of travel distance observed in the open-field test, further verifying that PR-SSS achieves central detoxification mainly via modulation of the tryptophan metabolic pathway. The changes in the tryptophan metabolic pathway and the neurotransmitters detected in this study are shown in Figure 9.

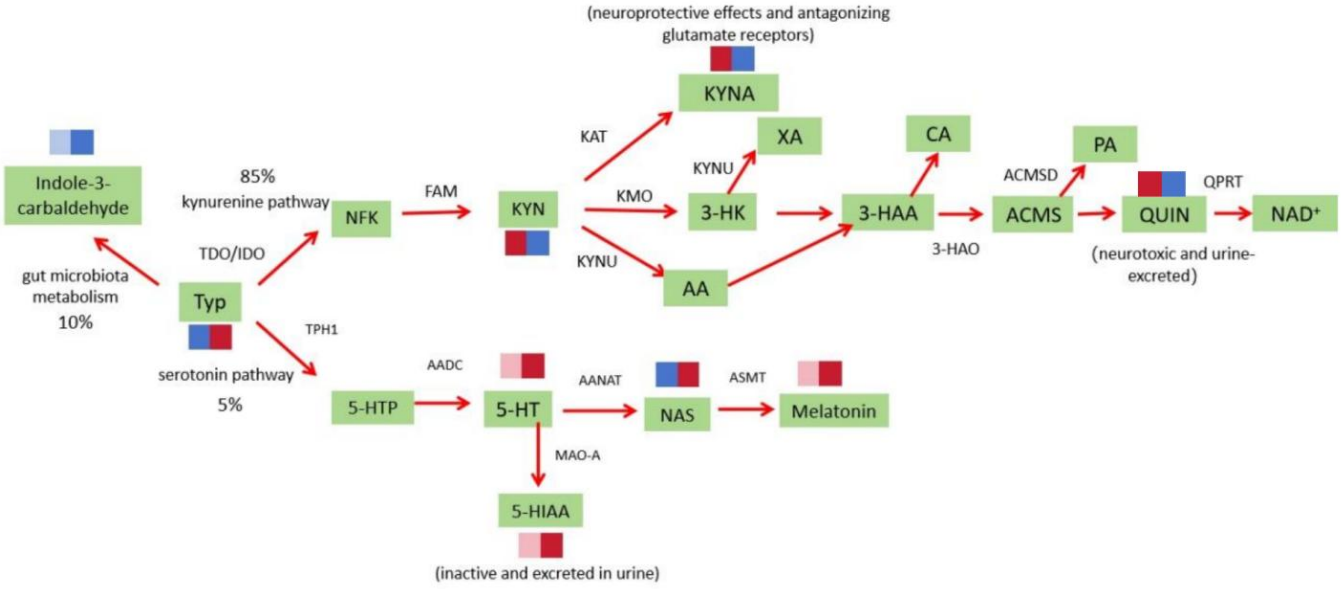

Figure 9. Tryptophan metabolic pathway schematic diagram Abbreviations: tryptophan (Trp), N-formylkynurenine (NFK) , kynurenin (KYN）, kynurenic acid (KYNA）, 3-hydroxynurenine (3-HK）, anthranilic acid (AA）, xanthurenic acis (XA）, 3-hydroxyanthranilic acid (3-HAA）, Cinnabarinic Acid (CA）, 2-amino-3-carboxymuconic acid-6-semialdehyde (ACMS）, Picolinic Acid (PA）, quinolinic acid (QUIN）, Nicotinamide Adenine Dinucleotide (NAD+）, 5-Hydroxytryptophan (5-HTP）, 5-hydroxytryptamine (5-HT）, 5-Hydroxyindole-3-acetic acid (5-HIAA）, N-Acetylserotonin (NAS）, Tryptophan 2,3-dioxygenase (TDO）, indoleamine 2,3-dioxygenase (IDO）, N-formylkynurenine

formamidase (FAM), kynurenine aminotransferase (KAT), kynurenine 3-monooxygenase (KMO), kynureninase (KYNU), 3-hydroxyanthranilate 3,4-dioxygenase (3-HAO),2-Amino-3-carboxymuconate-6-semialdehyde decarboxylase (ACMSD), quinolinate phosphoribosyltransferase (QPRT), Tryptophan hydroxylase 1 (TPH1), Aromatic-L-Amino-Acid Decarboxylase (AADC), aralkylamine N-acetyltransferase (AANAT), acetylserotonin O-methyltransferase (ASMT), Monoamine Oxidase-A (MAO-A).

Within the tryptophan metabolic pathway, the kynurenine branch represents the predominant route for tryptophan catabolism. Indoleamine 2,3-dioxygenase 1 (IDO1) is the initial rate-limiting enzyme mediating the conversion of tryptophan to kynurenine in the kynurenine pathway [15]. As the major isoform, IDO1 can be induced by pro-inflammatory cytokines such as IFN-γ, is widely distributed in nerve cells, and serves as a key target for drug development. IDO2 plays a relatively secondary role, and its detailed immunoregulatory mechanism remains under investigation [16]. Tryptophan 2,3-dioxygenase (TDO) is predominantly expressed in the liver and acts as the principal enzyme responsible for hepatic tryptophan degradation, which catalyzes the transformation of tryptophan (Trp) into N′-formylkynurenine (NFK) [17]. Kynurenine aminotransferase (KAT) catalyzes the transamination reaction between kynurenine and α-ketoglutarate to produce kynurenic acid and glutamate. Kynurenic acid exerts neuroprotective effects via glutamate-receptor antagonism [18-21]. 3-Hydroxykynurenine is generated through the hydroxylation of L-kynurenine catalyzed by kynurenine 3-monooxygenase (KMO), and is subsequently converted into 3-HAA. The latter is further transformed into ACMS under the catalysis of 3-HAO. ACMS can spontaneously convert into quinolinic acid in a non-enzymatic manner [22]. Quinolinic acid possesses multiple biological properties including neurotoxicity [23], glutamate-receptor-stimulating activity [24], pro-inflammatory effects [25], cell-death-inducing capacity [26-28], oxidative-stress-promoting activity [29], as well as regulatory impacts on cognitive function [30-33].

In the serotonin-melatonin metabolic pathway, serotonin and melatonin are crucial bioactive components. Tryptophan hydroxylase 1 (TPH1), also known as TPRH or TPH, catalyzes the conversion of tryptophan into 5-hydroxytryptophan [34]. Subsequently, 5-hydroxytryptophan is transformed into serotonin by aromatic-L-amino-acid decarboxylase (AADC), also referred to as DDC [35-38]. Serotonin undergoes two metabolic routes: one pathway converts serotonin into N-acetyl-5-hydroxytryptamine under the catalysis of aralkylamine N-acetyltransferase (AANAT), alternatively named SNAT [39]; the other pathway produces biologically-inactive 5-hydroxyindole-3-acetic acid via monoamine oxidase-A (MAO-A), which is eventually excreted in urine [40]. N-acetyl-5-hydroxytryptamine is then catalyzed by acetylserotonin O-methyltransferase (ASMT) to generate melatonin, an essential neurotransmitter for circadian rhythm regulation [41]. Supplemented serotonin and melatonin exert neuroprotective effects [12]. Serotonin can induce satiety, reduce pain sensitivity, suppress aggressive behavior, as well as regulate fatigue and provide neuroprotection [42]. As a potent antioxidant, melatonin interacts with a variety of reactive oxygen species (ROS) and reactive nitrogen species (RNS) via its indole moiety, which acts as the reaction-active site. Multiple downstream metabolites are thus produced, among which 6-hydroxymelatonin, 3-hydroxymelatonin, N1-acetyl-N2-formyl-5-methoxykynuramine and N1-acetyl-5-methoxykynuramine exhibit antioxidant capacity and are capable of scavenging up to four kinds of reactive oxygen species [43-44].

The molecular docking results revealed that the newly-generated compounds including Oliveramine, Scroneoside A, Cimicifugamide, Picrasidine C and 13-11 exhibited favorable binding energies and docking conformations with key enzymes in the tryptophan metabolic pathway, namely IDO1, TDO, TPH1, KAT, KMO, AADC, AANAT and ASMT. Therefore, we concluded that PR-SSS exerts its detoxifying effect against the central-nervous-system toxicity induced by SSS via compounds such as Oliveramine that target the enzymes of the tryptophan metabolic pathway. Further experimental verification and confirmation will be carried out in follow-up studies.

5. Conclusions

After processing with PR, slices of SSS at the same dosage produced lower acute toxicity in mice and sub-chronic neurotoxicity in rats. The integrated analysis of multi-omics differential metabolites and molecular-docking results revealed

that the mechanism underlying the reduced central-nervous-system toxicity involved down-regulation of the tryptophan-kynurenine pathway and up-regulation of the tryptophan-serotonin-melatonin pathway. This metabolic shift decreased the cerebral levels of neurotoxic constituents such as kynurenine and quinolinic acid, and increased the contents of neuroprotective substances including serotonin and melatonin in brain tissue, thereby partially protecting against the neuronal injury induced by SSS.

Supplementary Materials: The following supporting information presented in Table S1-S3.

Author Contributions: Yi Sui: Pharmacological experiments, omics experiments, article writing. Guo Feng: Article Structure and Methodology Guidance. Gang Liu, Minggang Teng: Chemical analysis, Xiaojie Hou, Li Zhang, Zhimin Lv: Methodological Experiment, Shiqiong Qin, : Metabolomics analysis, Yunli Wei, Xinping Wei: Transcriptomic analysis, Wei Li, Xiangling Qu, Yongyue Gao: Data Cleaning and Analysis, Qian Qin, Jinxi Wang, Sibu Ma: Article Chart Creation.

Funding: This work was supported by the Guizhou Province Special Science and Technology Research Project on Traditional Chinese Medicine and Ethnic Medicine (No. QZYY-2026-017), the Guizhou Provincial Forestry Bureau Key Project (No. Qian Lin Ke He Key Project [2026] 007), the National and Provincial Science and Technology Innovation Talent Team Cultivation Project of Guizhou University of Traditional Chinese Medicine (No. Guizhong Medicine TD He Zi [2024] 001), the "Thousand" Level Innovative Talents Project in Guizhou Province (No. Qrlf [2020] 4), the Guizhou University of Traditional Chinese Medicine ("Thousand Level" Talent) Research Project (No. ZQ2018001), the Guizhou Traditional Chinese Medicine Processing Technology Inheritance Base Construction Project (No. Qian Traditional Chinese Medicine Letter [2024] No. 22), the Guizhou Key Laboratory of Miao Medicine (No. ZSYS [2025] 018), the 2024 Guizhou Provincial Enterprise "Science and Technology Deputy Positions" and "Science and Technology Commissioners" Project (No. Qian Ke He Ren Cai KJZY [2025] 060). and the National Project for the Development of Inheritance Studios for Veteran TCM Pharmaceutical Technicians (Letter No. [2024] 255, NATCM HR & Education Dept.).

Institutional Review Board Statement: All experimental procedures complied with the animal experimentation ethics guidelines of Guizhou University of Traditional Chinese Medicine (Ethics Application No.: 20241118002).

Data Availability Statement: The original contributions presented in this study are included within the manuscript and supplementary materials. Please contact the corresponding author should you have any further questions.

Acknowledgments: All authors have reviewed and edited the manuscript and take full responsibility for the content of this publication.Conflicts of Interest: The authors declare no conflicts of interest.

Abbreviations

The following abbreviations are used in this manuscript:

SS	Strychni Semen
SSS	Sand-fried Strychni Semen
PR	Polygalae Radix
PR-SSS	Polygalae Radix-processed Sand-fried Strychni Semen

Appendix

Table S1 Compounds detected in SSS, Number range:(a)1-(a)40

No.(a)	Components	Molecular formula	molecular mass/Da	RT/min	response value	m/z	ppm	Adduct	Ion mode
1	2-Hydroxyfuran-3-carboxylic acid	C5H4O4	128.01	38.43	6118.00	128.01	-2.4	+e	$[M+H]^-$

2	Methyl succinate	C6H10O4	146.06	0.65	3121.00	191.06	4.9	+HCOO	$[M+H]^-$
	Methyl succinate	C6H10O4	146.06	3.06	6998.00	191.06	4.6	+HCOO	$[M+H]^-$
3	Methyl benzoate	C8H8O2	136.05	6.41	5362.00	135.05	7.3	-H	$[M+H]^-$
4	cis-Caffeic acid	C9H8O4	180.04	3.40	5598.00	179.04	5.7	-H	$[M+H]^-$
5	trans-Ferulaldehyde	C10H10O3	178.06	2.75	179.07	7058.00	8.6	+H	$[M+H]^+$
6	Methyl 1,4α,5,7α-tetrahydro-7-hydroxymethyl-cyclopenta[c]pyran-4-carboxylate	C10H12O4	196.07	2.74	197.08	5162.00	7.7	+H	$[M+H]^+$
7	Catalpol	C15H22O10	362.12	2.73	16880.00	421.14	0.2	+CH3COO, +HCOO	$[M+H]^-$
8	l-Pentadecene	C15H30	210.23	28.52	10421.00	255.23	3.3	+HCOO	$[M+H]^-$
9	Penniclavine	C16H18N2O2	270.14	14.68	21674.00	269.13	9.5	-H	$[M+H]^-$
	1-O-Caffeoylquinic acid	C16H18O9	354.10	0.64	22487.00	353.09	2.3	-H	$[M+H]^-$
10	1-O-Caffeoylquinic acid	C16H18O9	354.10	1.94	32686.00	353.09	1.8	-H	$[M+H]^-$
	1-O-Caffeoylquinic acid	C16H18O9	354.10	3.22	61413.00	353.09	1.9	-H	$[M+H]^-$
11	Sweroside	C16H22O9	358.13	4.61	4002.00	417.14	0.4	+CH3COO, -H	$[M+H]^-$
12	Mudanpioside F	C16H24O8	344.15	28.52	3203.00	403.16	5.9	+CH3COO	$[M+H]^-$
13	Methyl pentadecanoate	C16H32O2	256.24	15.10	274.28	8578.00	4.4	#REF!	$[M+H]^+$
	Methyl pentadecanoate	C16H32O2	256.24	15.41	274.28	4201.00	4.8	#REF!	$[M+H]^+$
14	Riboflavin	C17H20N4O6	376.14	0.61	415.10	34924.00	-0.3	+K, +Na	$[M+H]^+$
	Riboflavin	C17H20N4O6	376.14	0.65	80059.00	375.13	-1.3	-H, +CH3COO, +Cl, +HCOO	$[M+H]^-$
	Riboflavin	C17H20N4O6	376.14	2.73	366594.00	375.13	-1.2	-H, +Cl, +HCOO	$[M+H]^-$
15	Isofraxidin glycoside	C17H20O10	384.11	2.74	9655.00	443.12	-6.3	+CH3COO	$[M+H]^-$
16	Rehmannioside A	C17H26O10	390.15	4.20	20253.00	435.15	0.4	+HCOO, +Cl	$[M+H]^-$
17	1-Heptadecene	C17H34	238.27	31.43	3175.00	283.27	2.7	+HCOO	$[M+H]^-$
18	Mannotriose	C18H32O16	504.17	0.59	20079.00	549.17	-0.5	+HCOO, -H, +Cl	$[M+H]^-$
	Mannotriose	C18H32O16	504.17	0.59	543.13	16427.00	0.8	+K, +Na	$[M+H]^+$
19	Glyceryl monopalmitate	C19H38O4	330.28	26.21	331.29	26174.00	3.5	+H, +Na	$[M+H]^+$
	Glyceryl monopalmitate	C19H38O4	330.28	26.73	331.29	20042.00	3.8	+H, +Na	$[M+H]^+$

20	Glyceryl monopalmitate	C20H40O4	344.29	29.62	6998.00	403.31	-0.5	+CH3COO	$[M+H]^-$
21	Dihydrochelerythrine	C21H19NO4	349.13	4.68	367.17	3681.00	2.8	+NH4, +H	$[M+H]^+$
22	Strychnine	C21H22N2O2	334.17	0.68	335.18	35581.00	4.6	+H	$[M+H]^+$
	Strychnine	C21H22N2O2	334.17	4.32	335.18	867697.00	6.5	+H	$[M+H]^+$
23	Pseudostrychnine	C21H22N2O3	350.16	5.10	351.17	3748.00	2.5	+H	$[M+H]^+$
24	β-Glyceryl stearate	C21H42O4	358.31	29.51	359.32	38568.00	3.3	+H, +Na	$[M+H]^+$
	β-Glyceryl stearate	C21H42O4	358.31	30.05	359.32	30365.00	3.1	+H, +Na	$[M+H]^+$
25	Wogonoside	C22H20O11	460.10	0.61	4807.00	459.09	-5.2	-H	$[M+H]^-$
26	cis-head-to-head-3,3',4,4'-Limettin dimer	C22H20O8	412.12	0.63	14373.00	411.11	-4.3	-H	$[M+H]^-$
	cis-head-to-head-3,3',4,4'-Limettin dimer	C22H20O8	412.12	2.73	6408.00	411.11	-5.5	-H, +HCOO	$[M+H]^-$
27	Pseudostrychnine	C22H24N2O4	380.17	5.26	381.18	39584.00	3.0	+H	$[M+H]^+$
	Pseudostrychnine	C22H24N2O4	380.17	5.49	381.18	21397.00	3.1	+H	$[M+H]^+$
28	Senkyunolide	C22H30O2	326.22	5.12	365.19	84520.00	-1.5	+K	$[M+H]^+$
29	Andromedotoxin	C22H36O7	412.25	29.91	3829.00	412.25	6.4	+e	$[M+H]^-$
30	Dihydrochelerythrine	C22H41NO	335.32	4.30	335.32	5436.00	2.9	-e	$[M+H]^+$
31	Brucine	C23H26N2O4	394.19	0.64	395.20	112494.00	3.4	+H, +K	$[M+H]^+$
	Brucine	C23H26N2O4	394.19	3.90	8248.00	439.19	0.2	+HCOO, +Cl	$[M+H]^-$
	Brucine	C23H26N2O4	394.19	4.68	395.20	1159329.00	3.9	+H	$[M+H]^+$
32	Terrestribisamide	C24H28N2O6	440.19	4.33	11199.00	499.21	-0.3	+CH3COO	$[M+H]^-$
33	Bufotalinin	C24H30O6	414.20	16.29	5623.00	459.20	-0.8	+HCOO, +Cl	$[M+H]^-$
	Bufotalinin	C24H30O6	414.20	16.40	415.21	60297.00	2.0	+H, +Na, +NH4	$[M+H]^+$
	Bufotalinin	C24H30O6	414.20	16.72	415.21	24371.00	2.0	+H, +Na, +NH4	$[M+H]^+$
34	Bufalin	C24H34O4	386.25	4.61	425.21	5564.00	-2.6	+K	$[M+H]^+$
35	Andrographoside	C26H40O8	480.27	32.14	481.28	3576.00	8.1	+H	$[M+H]^+$
36	Mahuannin F	C30H22O10	542.12	0.70	12230.00	601.13	-9.5	+CH3COO, +Cl	$[M+H]^-$
37	Galloyl-oxypaeoniflorin	C30H32O16	648.17	3.14	6659.00	707.18	-2.5	+CH3COO	$[M+H]^-$
38	Marsdenoside G	C40H62O13	750.42	4.72	789.38	58987.00	1.9	+K	$[M+H]^+$

39	Periplogenoside K	C40H66O16	802.44	33.87	16571.00	802.43	-6.6	+e	$[M+H]^-$
40	Curculigosaponin G	C42H70O13	782.48	34.15	3233.00	817.45	-6.1	+Cl	$[M+H]^-$

712

Table S2 Compounds detected in PR-SSS, Number range:(b)1-(b)103 713

No.(b)	Components	Molecular formula	molecular mass/Da	RT/min	response value	m/z	ppm	Adduct	Ion mode
1	Inosine	C10H12N4O5	268.08	0.64	3283.00	327.09	-3.5	+CH3COO, -H	$[M+H]^-$
2	Myristicin	C11H12O3	192.08	8.37	3201.00	237.08	3.1	+HCOO	$[M+H]^-$
3	Maltose	C12H22O11	342.12	0.61	26682.00	341.11	2.0	-H, +Cl, +HCOO	$[M+H]^-$
	Maltose	C12H22O11	342.12	0.60	381.08	19503.00	3.7	+K, +Na	$[M+H]^+$
4	Catalpol	C15H22O10	362.12	2.74	9621.00	421.14	0.5	+CH3COO, +HCOO	$[M+H]^-$
5	L-Pentadecene	C15H30	210.23	28.53	11231.00	255.23	3.1	+HCOO	$[M+H]^-$
	L-Pentadecene	C15H30	210.23	29.00	7204.00	255.23	3.4	+HCOO	$[M+H]^-$
6	Brazilide A	C16H14O7	318.07	0.61	14658.00	377.09	-4.3	+CH3COO	$[M+H]^-$
7	Penniclavine	C16H18N2O2	270.14	14.73	19960.00	269.13	9.0	-H	$[M+H]^-$
8	1-O-Caffeoylquinic acid	C16H18O9	354.10	0.63	14435.00	353.09	1.6	-H	$[M+H]^-$
	1-O-Caffeoylquinic acid	C16H18O9	354.10	1.94	22340.00	353.09	2.0	-H	$[M+H]^-$
	1-O-Caffeoylquinic acid	C16H18O9	354.10	3.21	46060.00	353.09	1.9	-H	$[M+H]^-$
9	Toosendanoside A	C16H24O10	376.14	0.62	415.10	4542.00	1.3	+K	$[M+H]^+$
10	Methyl pentadecanoate	C16H32O2	256.24	15.05	274.28	10689.00	5.2	#REF!	$[M+H]^+$
	Methyl pentadecanoate	C16H32O2	256.24	15.36	274.28	5388.00	4.5	#REF!	$[M+H]^+$
11	Riboflavin	C17H20N4O6	376.14	0.62	39435.00	375.13	-2.3	-H, +CH3COO, +Cl, +HCOO	$[M+H]^-$
	Riboflavin	C17H20N4O6	376.14	1.53	36190.00	375.13	-1.8	-H	$[M+H]^-$
	Riboflavin	C17H20N4O6	376.14	2.75	235794.00	375.13	-1.3	-H, +Cl, +HCOO	$[M+H]^-$
12	Isofraxidin glycoside	C17H20O10	384.11	2.79	5465.00	443.12	-5.6	+CH3COO	$[M+H]^-$
13	Methyl chlorogenate	C17H20O9	368.11	7.01	369.12	7910.00	3.2	+H	$[M+H]^+$
14	Methyl 3-O-glucosyl-5-methoxy-trans-cinnamate	C17H22O9	370.13	7.65	4601.00	429.14	0.0	+CH3COO	$[M+H]^-$

15	1-Heptadecene	C17H34	238.27	31.38	3239.00	283.27	2.9	+HCOO	$[M+H]^-$
16	3-O-Acetyl-2-O-feruloyl-α-L-rhamnose	C18H22O9	382.13	7.92	383.13	9509.00	1.6	+H	$[M+H]^+$
17	10-O-Acetylgeniposidic acid	C18H24O11	416.13	2.33	3862.00	461.13	0.5	+HCOO	$[M+H]^-$
	10-O-Acetylgeniposidic acid	C18H24O11	416.13	3.65	3182.00	475.15	-0.1	+CH3COO	$[M+H]^-$
18	Mannotriose	C18H32O16	504.17	0.59	14989.00	549.17	-0.1	+HCOO, -H	$[M+H]^-$
	Mannotriose	C18H32O16	504.17	0.60	543.13	5666.00	0.9	+K, +Na	$[M+H]^+$
19	Sanleng acid	C18H34O5	330.24	11.82	10160.00	329.23	1.8	-H	$[M+H]^-$
20	Glyceryl monopalmitate	C19H38O4	330.28	26.20	331.29	17179.00	3.2	+H, +Na	$[M+H]^+$
	Glyceryl monopalmitate	C19H38O4	330.28	26.71	331.29	12913.00	3.4	+H, +Na	$[M+H]^+$
21	α-Hexadecylglyceryl ether	C19H40O3	316.30	38.00	339.29	3208.00	9.7	+Na	$[M+H]^+$
22	Oliveramine	C20H20N2O4	352.14	0.61	23204.00	387.11	8.0	+Cl	$[M+H]^-$
23	Morusin M-3′-O-β-D-glucopyranoside	C20H20O9	404.11	0.70	20495.00	439.08	-7.5	+Cl	$[M+H]^-$
24	Glyceryl monopalmitate	C20H40O4	344.29	29.64	5677.00	403.31	-0.2	+CH3COO	$[M+H]^-$
25	Strychnine	C21H22N2O2	334.17	0.69	335.18	19757.00	3.9	+H	$[M+H]^+$
	Strychnine	C21H22N2O2	334.17	4.32	335.18	556225.00	4.9	+H	$[M+H]^+$
26	Zhanjianlongoside A	C21H28O12	472.16	0.61	4748.00	517.16	-0.2	+HCOO	$[M+H]^-$
	Zhanjianlongoside A	C21H28O12	472.16	3.35	23597.00	517.16	-0.3	+HCOO	$[M+H]^-$
	Zhanjianlongoside A	C21H28O12	472.16	4.20	3188.00	517.16	-0.6	+HCOO, +CH3COO	$[M+H]^-$
27	Cistanoside F	C21H28O13	488.15	0.61	4333.00	547.17	-2.2	+CH3COO	$[M+H]^-$
	Cistanoside F	C21H28O13	488.15	3.60	21248.00	547.17	-0.5	+CH3COO	$[M+H]^-$
	Cistanoside F	C21H28O13	488.15	4.38	10551.00	547.17	-0.3	+CH3COO	$[M+H]^-$
28	β-Glyceryl stearate	C21H42O4	358.31	29.52	359.32	24013.00	3.3	+H, +Na	$[M+H]^+$
	β-Glyceryl stearate	C21H42O4	358.31	30.06	359.32	16811.00	3.0	+H, +Na	$[M+H]^+$
29	cis-head-to-head-3,3′,4,4′-Limettin dimer	C22H20O8	412.12	2.75	3866.00	411.11	-4.9	-H, +HCOO	$[M+H]^-$
	cis-head-to-head-3,3′,4,4′-Limettin dimer	C22H20O8	412.12	9.70	413.12	5026.00	0.7	+H	$[M+H]^+$
30	cis-head-to-head-3,3′,4,4′-Limettin dimer	C22H20O8	412.12	10.59	413.12	19427.00	1.5	+H	$[M+H]^+$
31	Nepitrin	C22H22O12	478.11	4.99	25419.00	537.12	-0.7	+CH3COO	$[M+H]^-$
	Pseudostrychnine	C22H24N2O4	380.17	5.25	381.18	15781.00	3.6	+H	$[M+H]^+$

	Pseudostrychnine	C22H24N2O4	380.17	5.49	381.18	13766.00	3.5	+H	$[M+H]^+$
32	Senkyunolide	C22H30O2	326.22	5.12	365.19	53672.00	-1.2	+K	$[M+H]^+$
33	Myricetin 3′,5′-dimethyl ether-3-O-β-D-glucopyranoside	C23H24O13	508.12	5.42	55083.00	567.14	-0.8	+CH3COO	$[M+H]^+$
	Brucine	C23H26N2O4	394.19	3.90	4396.00	439.19	0.0	+HCOO	$[M+H]^+$
34	Brucine	C23H26N2O4	394.19	0.65	395.20	66489.00	3.4	+H, +K	$[M+H]^+$
	Brucine	C23H26N2O4	394.19	4.68	395.20	752270.00	3.0	+H	$[M+H]^+$
35	Terrestribisamide	C24H28N2O6	440.19	4.34	5794.00	499.21	0.0	+CH3COO	$[M+H]^+$
	Bufotalinin	C24H30O6	414.20	16.33	7656.00	459.20	-0.2	+HCOO, +Cl	$[M+H]^+$
36	Bufotalinin	C24H30O6	414.20	16.32	415.21	71553.00	2.2	+H, +Na, +NH4, +K	$[M+H]^+$
	Bufotalinin	C24H30O6	414.20	16.61	415.21	33122.00	1.9	+H, +Na	$[M+H]^+$
37	Bufalin	C24H34O4	386.25	4.62	425.21	3438.00	-4.0	+K	$[M+H]^+$
38	Nystose	C24H42O21	666.22	0.58	3697.00	711.22	-1.7	+HCOO, -H	$[M+H]^+$
39	Neocoptiside A	C25H28O11	504.16	0.61	5352.00	539.13	-3.8	+Cl	$[M+H]^+$
40	Polygalaxanthone III	C25H28O15	568.14	5.49	569.15	4858.00	-0.6	+H	$[M+H]^+$
41	Cimicifugamide	C25H31NO10	505.19	0.62	12017.00	540.17	6.7	+Cl	$[M+H]^+$
42	Andrographoside	C26H40O8	480.27	32.15	481.28	3378.00	7.8	+H	$[M+H]^+$
43	Pinocembrin-7-neohesperidoside	C27H30O13	562.17	7.80	4844.00	621.18	-2.2	+CH3COO	$[M+H]^+$
44	Daidzein-4′,7-di-O-glucoside	C27H30O14	578.16	6.02	3303.00	637.18	-1.5	+CH3COO	$[M+H]^+$
45	Neoeriocitrin	C27H32O15	596.17	9.12	4252.00	641.17	-1.7	+HCOO, -H, +Cl	$[M+H]^+$
46	5α,8α-Epidioxy-(24R)-24-methylcholesta-6,9(11),22-trien-3β-ol	C28H42O3	426.31	11.83	3885.00	425.31	-0.1	-H, +HCOO	$[M+H]^+$
47	Picrasidine C	C29H26N4O4	494.20	0.63	6067.00	539.20	7.3	+HCOO	$[M+H]^+$
48	Olibanumol I	C29H48O2	428.37	35.09	429.37	3192.00	1.4	+H	$[M+H]^+$
49	(3,4,5-trihydroxy-6-(1,3,7-trihydroxy-9-oxo-9H-xanthen-2-yl)tetrahydro-2H-pyran-2-yl)methyl (E)-3-(3,4-dimethylphenyl)acrylate	C30H28O11	564.16	3.35	7822.00	563.16	9.7	-H	$[M+H]^+$
50	Galloyl-oxypaeoniflorin	C30H32O16	648.17	3.13	4403.00	707.18	-2.3	+CH3COO	$[M+H]^+$
51	Lysionotin-7-O-[α-L-rhamnosyl-(1→6)]-β-D-glucoside	C30H36O16	652.20	6.66	3014.00	651.19	-1.7	-H	$[M+H]^+$

	Lysionotin-7-O-[α-L-rhamnosyl-(1→6)]-β-D-glucoside	C30H36O16	652.20	7.47	12983.00	651.19	-1.7	-H, +Cl	$[M+H]^-$
	Lysionotin-7-O-[α-L-rhamnosyl-(1→6)]-β-D-glucoside	C30H36O16	652.20	9.63	15815.00	711.21	-2.1	+CH3COO	$[M+H]^-$
	Polygalaside B	C30H36O17	668.20	5.22	5297.00	667.19	-2.8	-H	$[M+H]^-$
52									
	Polygalaside B	C30H36O17	668.20	5.91	18681.00	667.19	-1.6	-H, +Cl, +HCOO	$[M+H]^-$
	Picfeltarraegenin VI	C30H44O6	500.31	10.27	501.32	5818.00	-1.0	+H	$[M+H]^+$
	Picfeltarraegenin VI	C30H44O6	500.31	11.86	501.32	3470.00	-1.8	+H	$[M+H]^+$
53									
	Picfeltarraegenin VI	C30H44O6	500.31	14.07	501.32	4249.00	-1.7	+H	$[M+H]^+$
	Picfeltarraegenin VI	C30H44O6	500.31	14.75	501.32	5743.00	-0.9	+H	$[M+H]^+$
	Cuscutaside A	C31H36O16	664.20	6.24	9415.00	723.21	-2.3	+CH3COO	$[M+H]^-$
54									
	Cuscutaside A	C31H36O16	664.20	7.16	38357.00	723.21	-2.4	+CH3COO	$[M+H]^-$
55	Portulacamide D	C31H37NO17	695.21	0.62	4283.00	695.20	-5.3	+e	$[M+H]^-$
	Polygalaside A	C31H38O17	682.21	7.15	41543.00	681.20	-1.2	-H	$[M+H]^-$
56	Polygalaside A	C31H38O17	682.21	7.86	182891.00	681.20	-0.9	-H, +CH3COO, +Cl, +HCOO	$[M+H]^-$
	Polygalaside A	C31H38O17	682.21	8.89	9087.00	681.20	-2.0	-H, +HCOO	$[M+H]^-$
57	Prunose I	C31H38O18	698.21	7.62	4535.00	697.20	-1.9	-H	$[M+H]^-$
	Parishin B	C32H40O19	728.22	7.85	21966.00	727.21	-2.5	-H	$[M+H]^-$
58									
	Parishin B	C32H40O19	728.22	8.89	4337.00	727.21	-2.7	-H, +CH3COO	$[M+H]^-$
	Grosvenorine	C33H40O19	740.22	6.94	38874.00	799.23	-2.2	+CH3COO, +HCOO	$[M+H]^-$
59									
	Grosvenorine	C33H40O19	740.22	7.85	3221.00	799.23	-2.9	+CH3COO	$[M+H]^-$
60	Nigelloside	C33H40O21	772.21	7.84	3421.00	771.19	-7.3	-H	$[M+H]^-$
61	Naringenin-4′-glucoside-7-rutinoside	C33H42O19	742.23	9.91	30066.00	741.22	-1.8	-H	$[M+H]^-$
62	(+)-Eucomminol di-O-glucopyranoside	C33H44O17	712.26	8.72	7088.00	747.22	-5.2	+Cl	$[M+H]^-$
	α-D-(6-O-Sinapoyl)-glucopyranosyl-(1→2)-β-D-(3-O-sinapoyl)-fructofuranoside	C34H42O19	754.23	0.63	6850.00	753.22	-1.9	-H, +CH3COO, +HCOO	$[M+H]^-$
63									
	α-D-(6-O-Sinapoyl)-glucopyranosyl-(1→2)-β-D-(3-O-sinapoyl)-fructofuranoside	C34H42O19	754.23	5.94	46815.00	753.22	-2.0	-H, +Cl	$[M+H]^-$

	α-D-(6-O-Sinapoyl)-glucopyranosyl-(1→2)-β-D-(3-O-sinapoyl)-fructofuranoside	C34H42O19	754.23	6.95	210441.00	753.22	-1.2	-H, +Cl, +HCOO	$[M+H]^-$
	α-D-(6-O-Sinapoyl)-glucopyranosyl-(1→2)-β-D-(3-O-sinapoyl)-fructofuranoside	C34H42O19	754.23	7.84	5473.00	753.22	-2.8	-H, +HCOO	$[M+H]^-$
	α-D-(6-O-Sinapoyl)-glucopyranosyl-(1→2)-β-D-(3-O-sinapoyl)-fructofuranoside	C34H42O19	754.23	8.80	14104.00	813.24	-3.3	+CH3COO	$[M+H]^-$
64	Isorhamnetin-3-O-(2G-α-L-rhamnosyl)-rutinoside	C34H42O20	770.23	7.15	7650.00	769.22	-1.8	-H, +HCOO	$[M+H]^-$
	Isorhamnetin-3-O-(2G-α-L-rhamnosyl)-rutinoside	C34H42O20	770.23	8.74	11300.00	770.23	-0.2	+e	$[M+H]^-$
	Polygalaside C	C35H44O19	768.25	7.75	6846.00	767.24	-3.3	-H	$[M+H]^-$
65	Polygalaside C	C35H44O19	768.25	8.80	38874.00	767.24	-2.5	-H, +Cl, +HCOO	$[M+H]^-$
66	15α-Hydroxycimigoside H2	C35H54O11	650.37	13.61	8760.00	649.36	-2.2	-H	$[M+H]^-$
67	Magnoflorine	C36H52O16	740.33	15.21	5253.00	799.34	-2.2	+CH3COO	$[M+H]^-$
68	Platycogenic acid A lactone	C36H54O12	678.36	11.54	7039.00	677.35	-2.4	-H, +HCOO	$[M+H]^-$
69	Phytolaccaside P	C36H56O12	680.38	11.83	156063.00	679.37	-1.2	-H, +Cl, +HCOO	$[M+H]^-$
	Neocuscutaside A	C37H46O21	826.25	3.29	3584.00	871.25	-3.4	+HCOO	$[M+H]^-$
70	Neocuscutaside A	C37H46O21	826.25	9.82	21941.00	825.24	-2.3	-H	$[M+H]^-$
71	Moracenin G	C40H36O11	692.23	9.10	4666.00	737.23	5.5	+HCOO	$[M+H]^-$
72	1,2′,4′,6′-Tetraacetyl-3,6-diferuloylsucrose	C40H46O21	862.25	12.97	4116.00	861.24	-3.6	-H	$[M+H]^-$
73	Marsdenoside G	C40H62O13	750.42	4.71	789.38	30784.00	1.0	+K	$[M+H]^+$
74	Periplogenoside K	C40H66O16	802.44	33.76	20813.00	802.43	-5.9	+e	$[M+H]^-$
75	Lyciumin A	C42H51N9O12	873.37	14.80	12259.00	918.37	8.9	+HCOO	$[M+H]^-$
76	3-O-Decanoyl-16-O-acetylisoiridogermanal	C42H70O6	670.52	29.60	11723.00	715.51	-8.5	+HCOO	$[M+H]^-$
77	Hookeroside D	C43H70O18	874.46	7.90	8235.00	873.45	-3.6	-H	$[M+H]^-$
78	Phytolaccaside I	C49H78O22	1018.50	9.80	8003.00	1017.49	-3.8	-H	$[M+H]^-$
79	Stauntonoside YM13	C51H80O21	1028.52	11.01	7715.00	1073.51	-4.9	+HCOO	$[M+H]^-$
80	Foetidissimoside A	C52H82O22	1058.53	10.20	272034.00	1103.52	-2.9	+HCOO	$[M+H]^-$

	Julibroside C1	C53H82O24	1102.52	10.11	7540.00	1101.51	-4.1	-H	[M+H]-
81									
	Julibroside C1	C53H82O24	1102.52	10.77	3669.00	1101.51	-4.6	-H	[M+H]-
82	Aster saponin Hc	C57H90O26	1190.57	10.04	58967.00	1235.57	-3.7	+HCOO	[M+H]-
83	Timosaponin I2 (Timosaponin D2)	C57H96O28	1228.61	15.94	5519.00	1263.57	-3.2	+Cl	[M+H]-
84	Timosaponin B-6	C58H98O29	1258.62	15.05	4290.00	1293.59	-2.7	+Cl	[M+H]-
85	2″-O-Acetylpolygalacin D	C59H94O28	1250.59	10.37	50709.00	1249.58	-4.0	-H	[M+H]-
86	Platycodin C	C59H94O29	1266.59	9.75	196654.00	1265.58	-3.3	-H	[M+H]-
87	2-Hydroxyfuran-3-carboxylic acid	C5H4O4	128.01	38.51	4510.00	128.01	-4.6	+e	[M+H]-
88	Vaccaroside B	C60H94O29	1278.59	15.39	12755.00	1323.60	6.8	+HCOO	[M+H]-
89	Aster saponin Hd	C62H98O30	1322.61	9.98	29407.00	1367.61	-3.8	+HCOO	[M+H]-
90	Tubeimoside II	C63H98O30	1334.61	10.27	42405.00	1379.61	-4.0	+HCOO	[M+H]-
91	Tubeimoside III	C64H100O31	1364.62	15.11	58582.00	1409.63	6.9	+HCOO	[M+H]-
92	Lobatoside I	C65H102O33	1410.63	14.71	56290.00	1469.65	6.5	+CH3COO	[M+H]-
93	2″-O-Acetylpolygalacin D2	C65H104O33	1412.65	9.97	16988.00	1411.63	-4.4	-H	[M+H]-
	Geniposidic acid tetramer acetate	C66H84O38	1484.46	7.89	8143.00	1483.45	-5.1	-H, +HCOO	[M+H]-
94	Geniposidic acid tetramer acetate	C66H84O38	1484.46	8.63	5643.00	1483.45	-5.4	-H, +Cl	[M+H]-
	Geniposidic acid tetramer acetate	C66H84O38	1484.46	10.02	5179.00	1483.45	-5.3	-H, +HCOO	[M+H]-
95	3-O-β-D-Galactopyranosyl-(1→2)-β-D-glucuro-nopyranosyl gypso-genin-28-O-β-D-xylopyra-nosyl-(1→4)-[β-D-6-O-acetyl glucopyra-nosyl-(1→3)]-α-L-rhamnopyra-nosyl-(1→2)-β-D-fucopyranoside	C67H104O34	1452.64	10.20	27093.00	1511.65	-4.1	+CH3COO	[M+H]-
	3-O-β-D-Galactopyranosyl-(1→2)-β-D-glucuro-nopyranosyl gypso-genin-28-O-β-D-xylopyra-nosyl-(1→4)-[β-D-6-O-acetyl glucopyra-nosyl-(1→3)]-α-L-rhamnopyra-nosyl-(1→2)-β-D-fucopyranoside	C67H104O34	1452.64	15.33	5218.00	1497.65	4.3	+HCOO	[M+H]-
96	Parthenocissin A	C68H52O44	1572.18	14.45	13513.00	1572.19	2.0	+e	[M+H]-
97	Methyl succinate	C6H10O4	146.06	3.07	5543.00	191.06	5.0	+HCOO	[M+H]-
	Polygalacin G	C70H104O32	1456.65	13.70	10765.00	1455.64	-4.9	-H, +HCOO	[M+H]-
98	Polygalacin G	C70H104O32	1456.65	14.40	19085.00	1455.64	-3.6	-H	[M+H]-
	Polygalacin G	C70H104O32	1456.65	15.00	82115.00	1455.64	-3.6	-H	[M+H]-

	3-O-β-D-Galactopyranosyl-(1→2)-β-D-glucuronopyranosyl-(1→3)-β-D-glucuronopyranosyl-gypsogenin-28-O-β-D-xylopyranosyl-(1→4)-[β-D-glucopyranosyl-(1→3)]-α-L-rhamnopyranosyl-(1→2)-β-D-fucopyranoside	C70H110O37	1542.67	9.81	15665.00	1541.66	-4.2	-H	[M+H]-
	3-O-β-D-Galactopyranosyl-(1→2)-β-D-glucuronopyranosyl-(1→3)-β-D-glucuronopyranosyl-gypsogenin-28-O-β-D-xylopyranosyl-(1→4)-[β-D-glucopyranosyl-(1→3)]-α-L-rhamnopyranosyl-(1→2)-β-D-fucopyranoside	C70H110O37	1542.67	12.90	3645.00	1587.68	4.1	+HCOO	[M+H]-
	3-O-β-D-Galactopyranosyl-(1→2)-β-D-glucuronopyranosyl-(1→3)-β-D-glucuronopyranosyl-gypsogenin-28-O-β-D-xylopyranosyl-(1→4)-[β-D-glucopyranosyl-(1→3)]-α-L-rhamnopyranosyl-(1→2)-β-D-fucopyranoside	C70H110O37	1542.67	13.83	34248.00	1601.69	3.6	+CH3COO	[M+H]-
99	3-O-β-D-Galactopyranosyl-(1→2)-β-D-glucuronopyranosyl-(1→3)-β-D-glucuronopyranosyl-gypsogenin-28-O-β-D-xylopyranosyl-(1→4)-[β-D-glucopyranosyl-(1→3)]-α-L-rhamnopyranosyl-(1→2)-β-D-fucopyranoside	C70H110O37	1542.67	14.62	51947.00	1541.67	5.9	-H	[M+H]-
	3-O-β-D-Galactopyranosyl-(1→2)-β-D-glucuronopyranosyl-(1→3)-β-D-glucuronopyranosyl-gypsogenin-28-O-β-D-xylopyranosyl-(1→4)-[β-D-glucopyranosyl-(1→3)]-α-L-rhamnopyranosyl-(1→2)-β-D-fucopyranoside	C70H110O37	1542.67	14.99	161725.00	1587.68	6.2	+HCOO	[M+H]-
	3-O-β-D-Galactopyranosyl-(1→2)-β-D-glucuronopyranosyl-(1→3)-β-D-glucuronopyranosyl-gypsogenin-28-O-β-D-xylopyranosyl-(1→4)-[β-D-glucopyranosyl-(1→3)]-α-L-rhamnopyranosyl-(1→2)-β-D-fucopyranoside	C70H110O37	1542.67	15.28	7142.00	1541.67	4.3	-H	[M+H]-
	Polygalacin E	C71H106O33	1486.66	13.55	10408.00	1485.65	-5.2	-H	[M+H]-
100	Polygalacin E	C71H106O33	1486.66	14.82	52463.00	1485.65	-3.7	-H	[M+H]-
	Polygalacin B	C75H112O35	1572.70	13.12	70664.00	1617.69	-4.6	+HCOO	[M+H]-
101	Polygalacin B	C75H112O35	1572.70	14.13	166369.00	1631.71	-3.8	+CH3COO	[M+H]-
	Polygalacin B	C75H112O35	1572.70	14.45	319674.00	1571.69	-3.2	-H, +HCOO	[M+H]-

	Polygalacin F	C75H112O36	1588.69	13.74	6990.00	1647.70	-4.8	+CH3COO	$[M+H]^+$
102	Polygalacin F	C75H112O36	1588.69	14.03	82070.00	1587.68	-3.9	-H	$[M+H]^+$
	Polygalacin F	C75H112O36	1588.69	14.99	133710.00	1588.68	-6.3	+e, -H	$[M+H]^+$
	Polygalacin A	C80H120O39	1704.74	13.94	174661.00	1703.73	-3.8	-H	$[M+H]^+$
103									
	Polygalacin A	C80H120O39	1704.74	14.14	105957.00	1749.73	-4.2	+HCOO	$[M+H]^+$

714

Table S3 Compounds detected in PR, Number range:(c)1-(c)123 715

No.(c)	Components	Molecular formula	molecular mass/Da	RT/min	response value	m/z	ppm	Adduct	Ion mode
1	Dihydrogentianine	C10H11NO2	177.08	0.68	200.07	3648.00	-1.6	+Na	$[M+H]^+$
2	Myristicin	C11H12O3	192.08	8.35	4323.00	237.08	2.9	+HCOO	$[M+H]^+$
3	E-3,4,5-trimethoxycinnamic acid	C12H14O5	238.08	3.20	6611.00	283.08	3.3	+HCOO	$[M+H]^+$
4	Prunasin	C14H17NO6	295.11	0.61	4062.00	295.10	-7.9	+e	$[M+H]^+$
5	Dencoryphin	C15H18O6	294.11	5.28	4281.00	339.11	1.2	+HCOO	$[M+H]^+$
6	Caffeic acid-β-D-glucopyranosyl ester glycoside	C15H18O9	342.10	4.51	8423.00	401.11	0.5	+CH3COO	$[M+H]^+$
7	l-Pentadecene	C15H30	210.23	28.53	10544.00	255.23	2.7	+HCOO	$[M+H]^+$
	l-Pentadecene	C15H30	210.23	28.99	6349.00	255.23	2.4	+HCOO	$[M+H]^+$
8	Penniclavine	C16H18N2O2	270.14	14.71	18908.00	269.13	8.7	-H	$[M+H]^+$
9	3-O-trans-coumaroylquinic acid	C16H18O8	338.10	3.37	339.11	3162.00	1.3	+H	$[M+H]^+$
10	4-O-p-methoxycinnamoyl-α-L-rhamnose	C16H20O7	324.12	5.40	8640.00	369.12	0.3	+HCOO	$[M+H]^+$
11	3-[(3-hydroxy)-(4-O-D-glucosyl)-phenyl]-2-propenoic acid	C16H20O9	356.11	6.73	3789.00	415.12	0.8	+CH3COO	$[M+H]^+$
12	Hexadecenoic acid	C16H30O2	254.22	15.97	8151.00	313.24	2.0	+CH3COO	$[M+H]^+$
13	Methyl pentadecanoate	C16H32O2	256.24	15.08	274.28	8171.00	4.3	#REF!	$[M+H]^+$
14	Methyl pentadecanoate	C16H32O2	256.24	15.36	274.28	5851.00	4.5	#REF!	$[M+H]^+$
15	3,5,3',4'-Tetrahydroxy-6,7-dimethoxyflavone	C17H14O8	346.07	4.61	3812.00	405.08	0.7	+CH3COO	$[M+H]^+$
16	Bergaptol-O-β-D-glucopyranoside	C17H16O9	364.08	0.60	365.09	6194.00	-2.6	+H	$[M+H]^+$
17	Methyl chlorogenate	C17H20O9	368.11	6.00	369.12	3719.00	1.1	+H	$[M+H]^+$
	Methyl chlorogenate	C17H20O9	368.11	7.01	369.12	19439.00	2.5	+H	$[M+H]^+$
18	Methyl 3-O-glucosyl-5-methoxy-trans-cinnamate	C17H22O9	370.13	7.63	8935.00	429.14	-0.4	+CH3COO	$[M+H]^+$
19	Ophiopogonflavone A	C18H14O6	326.08	12.01	3333.00	371.08	1.2	+HCOO	$[M+H]^+$
20	Abrusaquinone G	C18H18O8	362.10	0.62	4322.00	361.09	-4.9	-H	$[M+H]^+$
21	3-O-Acetyl-2-O-p-methoxycinnamoyl-α-L-rhamnose	C18H22O8	366.13	14.31	367.14	3385.00	1.2	+H	$[M+H]^+$
	3-O-Acetyl-2-O-p-methoxycinnamoyl-α-L-rhamnose	C18H22O8	366.13	15.17	367.14	4408.00	0.8	+H	$[M+H]^+$
22	3-O-Acetyl-2-O-feruloyl-α-L-rhamnose	C18H22O9	382.13	7.93	383.13	28500.00	3.0	+H	$[M+H]^+$

	3-O-Acetyl-2-O-feruloyl-α-L-rhamnose	C18H22O9	382.13	8.88	383.13	3820.00	0.0	+H	$[M+H]^+$
	3-O-Acetyl-2-O-feruloyl-α-L-rhamnose	C18H22O9	382.13	9.97	383.13	3372.00	0.4	+H	$[M+H]^+$
23	10-O-Acetylgeniposidic acid	C18H24O11	416.13	3.66	6093.00	475.15	-0.5	+CH3COO, +HCOO	$[M+H]^-$
24	Mannotriose	C18H32O16	504.17	0.62	3076.00	503.16	0.8	-H	$[M+H]^-$
25	Sanleng acid	C18H34O5	330.24	11.81	11940.00	329.23	2.1	-H	$[M+H]^-$
26	Gardenin E	C19H18O9	390.10	5.32	7152.00	435.09	0.4	+HCOO	$[M+H]^-$
27	4-Methoxybenzaldehyde-2-O-[β-D-xylo-syl-(1→6)-β-D-glucose]	C19H26O12	446.14	2.10	3137.00	491.14	-1.0	+HCOO	$[M+H]^-$
28	(10E,9S,12S,13S)-Trihydroxy-10-octadecen-oate	C19H36O5	344.26	1.58	9898.00	389.26	4.2	+HCOO	$[M+H]^-$
29	Glyceryl monopalmitate	C19H38O4	330.28	26.21	331.29	14774.00	2.3	+H, +Na	$[M+H]^+$
	Glyceryl monopalmitate	C19H38O4	330.28	26.72	331.28	10443.00	1.8	+H, +Na	$[M+H]^+$
30	α-Hexadecylglyceryl ether	C19H40O3	316.30	36.53	339.29	3953.00	6.2	+Na	$[M+H]^+$
31	3-Hydroxy-5,7,8,3',4'-pentamethoxyflavone	C20H20O8	388.12	0.70	5183.00	423.08	-9.1	+Cl	$[M+H]^-$
32	Glyceryl monopalmitate	C20H40O4	344.29	29.64	5108.00	403.31	0.6	+CH3COO	$[M+H]^-$
33	Dehydroglaucine	C21H23NO4	353.16	11.88	10034.00	388.13	-3.5	+Cl	$[M+H]^-$
	Zhanjianlongoside A	C21H28O12	472.16	0.61	9415.00	517.16	0.1	+HCOO	$[M+H]^-$
34	Zhanjianlongoside A	C21H28O12	472.16	3.35	55285.00	517.16	0.4	+HCOO	$[M+H]^-$
	Zhanjianlongoside A	C21H28O12	472.16	4.19	3484.00	517.16	-0.7	+HCOO	$[M+H]^-$
	Cistanoside F	C21H28O13	488.15	0.61	6478.00	547.17	-0.4	+CH3COO	$[M+H]^-$
35	Cistanoside F	C21H28O13	488.15	3.60	38784.00	547.17	-0.1	+CH3COO, -H	$[M+H]^-$
	Cistanoside F	C21H28O13	488.15	4.36	5764.00	547.17	-1.1	+CH3COO	$[M+H]^-$
	Cistanoside F	C21H28O13	488.15	6.96	3059.00	547.17	-0.5	+CH3COO	$[M+H]^-$
36	Rehmannioside A1	C21H32O15	524.17	0.62	8456.00	524.17	-2.7	+e	$[M+H]^-$
	Methyl 12-hydroxyhydroabietate	C21H36O3	336.27	30.61	337.27	3620.00	1.5	+H	$[M+H]^+$
	Methyl 12-hydroxyhydroabietate	C21H36O3	336.27	32.33	337.27	14730.00	3.0	+H	$[M+H]^+$
	Methyl 12-hydroxyhydroabietate	C21H36O3	336.27	32.62	337.28	14730.00	3.9	+H	$[M+H]^+$
37	Methyl 12-hydroxyhydroabietate	C21H36O3	336.27	33.64	337.28	10542.00	3.9	+H	$[M+H]^+$
	Methyl 12-hydroxyhydroabietate	C21H36O3	336.27	33.89	337.28	11066.00	4.5	+H	$[M+H]^+$
	Methyl 12-hydroxyhydroabietate	C21H36O3	336.27	34.23	337.28	8487.00	3.9	+H	$[M+H]^+$
	Methyl 12-hydroxyhydroabietate	C21H36O3	336.27	36.51	337.27	6454.00	2.1	+H	$[M+H]^+$
	Methyl 12-hydroxyhydroabietate	C21H36O3	336.27	37.74	337.27	4252.00	0.5	+H	$[M+H]^+$
38	β-Glyceryl stearate	C21H42O4	358.31	29.52	359.32	16576.00	2.6	+H, +Na	$[M+H]^+$
	β-Glyceryl stearate	C21H42O4	358.31	30.06	359.32	11021.00	1.9	+H, +Na	$[M+H]^+$
	cis-head-to-head-3,3',4,4'-Limettin dimer	C22H20O8	412.12	8.80	413.12	7811.00	1.5	+H	$[M+H]^+$
39	cis-head-to-head-3,3',4,4'-Limettin dimer	C22H20O8	412.12	9.67	413.12	25977.00	1.2	+H	$[M+H]^+$
	cis-head-to-head-3,3',4,4'-Limettin dimer	C22H20O8	412.12	10.58	413.12	55563.00	2.3	+H	$[M+H]^+$
	cis-head-to-head-3,3',4,4'-Limettin dimer	C22H20O8	412.12	11.36	413.12	4257.00	0.2	+H	$[M+H]^+$
40	Nepitrin	C22H22O12	478.11	5.00	59007.00	537.13	0.1	+CH3COO	$[M+H]^-$

41	Myricetin 3′,5′-dimethyl ether-3-O-β-D-glucopyranoside	C23H24O13	508.12	0.63	4533.00	567.14	-0.4	+CH3COO, +Cl	$[M+H]^-$
	Myricetin 3′,5′-dimethyl ether-3-O-β-D-glucopyranoside	C23H24O13	508.12	5.43	103554.00	567.14	-0.3	+CH3COO	$[M+H]^-$
42	Sibiricaxanthone A	C24H26O14	538.13	5.83	3726.00	597.15	1.5	+CH3COO	$[M+H]^-$
	Sibiricaxanthone A	C24H26O14	538.13	5.04	539.14	3522.00	-1.2	+H	$[M+H]^+$
43	Bufotalinin	C24H30O6	414.20	16.34	5920.00	459.20	-0.7	+HCOO, +Cl	$[M+H]^-$
	Bufotalinin	C24H30O6	414.20	16.34	415.21	52820.00	2.2	+H, +Na, +NH4, +K	$[M+H]^+$
44	Vitetrifolin D	C24H38O5	406.27	4.67	7790.00	451.27	3.2	+HCOO	$[M+H]^-$
45	Nystose	C24H42O21	666.22	0.58	3143.00	711.22	-0.5	+HCOO, -H	$[M+H]^-$
46	Polygalaxanthone III	C25H28O15	568.14	5.48	569.15	17230.00	-1.1	+H, +Na	$[M+H]^+$
47	Chasmanine	C25H41NO6	451.29	2.59	451.29	6007.00	-3.9	-e	$[M+H]^+$
48	Tetraacetylasperuloside	C26H30O15	582.16	6.66	6057.00	581.15	-1.3	-H, +HCOO	$[M+H]^-$
49	Pinocembrin-7-neohesperidoside	C27H30O13	562.17	7.80	10538.00	621.18	-1.6	+CH3COO	$[M+H]^-$
50	Daidzein-4′,7-di-O-glucoside	C27H30O14	578.16	6.03	7220.00	637.18	-1.5	+CH3COO	$[M+H]^-$
51	Neoeriocitrin	C27H32O15	596.17	7.98	3800.00	641.17	-2.1	+HCOO, -H, +Cl	$[M+H]^-$
	Neoeriocitrin	C27H32O15	596.17	9.12	8609.00	641.17	-1.9	+HCOO, -H, +Cl	$[M+H]^-$
52	(2R,3R)-Taxifolin-7-O-α-L-rhamnopyranosyl-(1→6)-β-D-glucopyranoside	C27H32O16	612.17	6.81	4119.00	611.16	-1.9	-H	$[M+H]^-$
	(2R,3R)-Taxifolin-7-O-α-L-rhamnopyranosyl-(1→6)-β-D-glucopyranoside	C27H32O16	612.17	9.60	4588.00	671.18	-3.5	+CH3COO	$[M+H]^-$
53	2"-O-Glucosylisoswertisin	C28H32O15	608.17	7.80	5495.00	667.19	-1.1	+CH3COO	$[M+H]^-$
54	5α,8α-Epidioxy-(24R)-24-methylcholesta-6,9(11),22-trien-3β-ol	C28H42O3	426.31	11.82	3150.00	425.31	0.5	-H, +HCOO	$[M+H]^-$
55	Malvidin-3,5-di-O-glucoside	C29H34O17	654.18	4.95	6451.00	699.18	-2.2	+HCOO, +CH3COO	$[M+H]^-$
56	Limocitrin-3,7-di-O-β-D-glucoside	C29H34O18	670.17	5.21	23019.00	729.19	-2.1	+CH3COO	$[M+H]^-$
57	3′,4′-Dimethoxy-7,2′-di-O-glucosylisoflavan glycoside	C29H38O15	626.22	9.11	4023.00	661.20	8.5	+Cl	$[M+H]^-$
58	Scutebarbatine C	C29H38O9	530.25	9.31	3545.00	589.27	4.3	+CH3COO	$[M+H]^-$
59	Olibanumol I	C29H48O2	428.37	34.45	429.37	3453.00	0.2	+H	$[M+H]^+$
60	Lysionotin-7-O-[α-L-rhamnosyl-(1→6)]-β-D-glucoside	C30H36O16	652.20	6.64	5381.00	651.19	-2.6	-H	$[M+H]^-$
	Lysionotin-7-O-[α-L-rhamnosyl-(1→6)]-β-D-glucoside	C30H36O16	652.20	7.47	26344.00	651.19	-2.1	-H, +Cl	$[M+H]^-$
	Lysionotin-7-O-[α-L-rhamnosyl-(1→6)]-β-D-glucoside	C30H36O16	652.20	9.62	25036.00	711.21	-1.8	+CH3COO	$[M+H]^-$

	Polygalaside B	C30H36O17	668.20	5.20	8920.00	667.19	-2.1	-H, +HCOO	$[M+H]^+$
61	Polygalaside B	C30H36O17	668.20	5.92	39381.00	667.19	-1.7	-H, +Cl, +HCOO	$[M+H]^+$
	Picfeltarraegenin VI	C30H44O6	500.31	9.82	501.32	3429.00	-1.5	+H	$[M+H]^+$
	Picfeltarraegenin VI	C30H44O6	500.31	10.28	501.32	16392.00	-0.3	+H	$[M+H]^+$
62	Picfeltarraegenin VI	C30H44O6	500.31	14.10	501.32	14529.00	-0.6	+H	$[M+H]^+$
	Picfeltarraegenin VI	C30H44O6	500.31	14.77	501.32	14412.00	-0.6	+H	$[M+H]^+$
	Cuscutaside A	C31H36O16	664.20	6.26	15292.00	723.21	-2.3	+CH3COO	$[M+H]^+$
63	Cuscutaside A	C31H36O16	664.20	7.16	80036.00	723.21	-1.9	+CH3COO	$[M+H]^+$
64	Tubuloside E	C31H38O15	650.22	7.44	3811.00	709.23	-3.3	+CH3COO	$[M+H]^+$
65	2′-Acetylacteoside	C31H38O16	666.22	7.72	3156.00	711.21	-2.0	+HCOO	$[M+H]^+$
66	Polygalaside A	C31H38O17	682.21	7.86	436897.00	681.20	-0.8	-H, +CH3COO, +Cl, +HCOO	$[M+H]^+$
	Polygalaside A	C31H38O17	682.21	8.89	9849.00	681.20	-1.7	-H, +HCOO	$[M+H]^+$
	Prunose I	C31H38O18	698.21	6.05	4227.00	697.20	-2.3	-H	$[M+H]^+$
67	Prunose I	C31H38O18	698.21	7.64	6826.00	697.20	-1.9	-H	$[M+H]^+$
	Prunose I	C31H38O18	698.21	10.38	4285.00	697.20	-0.4	-H	$[M+H]^+$
68	Semen-ziziphi-spinosae-alkaloid A	C31H42N4O4	534.32	9.19	557.31	4880.00	1.8	+Na	$[M+H]^+$
	Parishin B	C32H40O19	728.22	7.85	44481.00	727.21	-1.8	-H	$[M+H]^+$
69	Parishin B	C32H40O19	728.22	8.91	4238.00	727.21	-2.1	-H, +CH3COO	$[M+H]^+$
70	Grosvenorine	C33H40O19	740.22	6.94	74038.00	799.23	-2.0	+CH3COO, +HCOO	$[M+H]^+$
	Grosvenorine	C33H40O19	740.22	7.86	3437.00	799.23	-1.4	+CH3COO	$[M+H]^+$
71	Cerberin	C33H40O20	756.21	10.33	3480.00	756.22	9.5	+e	$[M+H]^+$
72	Nigelloside	C33H40O21	772.21	7.85	5563.00	771.20	-4.5	-H	$[M+H]^+$
73	Naringenin-4′-glucoside-7-rutinoside	C33H42O19	742.23	9.90	54800.00	741.22	-1.7	-H	$[M+H]^+$
74	(+)-Eucomminol di-O-glucopyranoside	C33H44O17	712.26	8.72	12398.00	747.22	-4.4	+Cl	$[M+H]^+$
	α-D-(6-O-Sinapoyl)-glucopyranosyl-(1→2)-β-D-(3-O-sinapoyl)-fructofuranoside	C34H42O19	754.23	0.64	10387.00	753.22	-1.6	-H, +Cl, +HCOO	$[M+H]^+$
	α-D-(6-O-Sinapoyl)-glucopyranosyl-(1→2)-β-D-(3-O-sinapoyl)-fructofuranoside	C34H42O19	754.23	5.97	77731.00	753.22	-2.0	-H, +Cl	$[M+H]^+$
75	α-D-(6-O-Sinapoyl)-glucopyranosyl-(1→2)-β-D-(3-O-sinapoyl)-fructofuranoside	C34H42O19	754.23	6.95	380129.00	753.22	-1.3	-H, +Cl, +HCOO	$[M+H]^+$
	α-D-(6-O-Sinapoyl)-glucopyranosyl-(1→2)-β-D-(3-O-sinapoyl)-fructofuranoside	C34H42O19	754.23	7.84	5275.00	753.22	-2.9	-H, +HCOO	$[M+H]^+$

	α-D-(6-O-Sinapoyl)-glucopyranosyl-(1→2)-β-D-(3-O-sinapoyl)-fructofuranoside	C34H42O19	754.23	8.80	27423.00	813.24	-2.7	+CH3COO	[M+H]-
76	Isorhamnetin-3-O-(2G-α-L-rhamnosyl)-rutinoside	C34H42O20	770.23	7.16	14606.00	769.22	-2.6	-H	[M+H]-
	Isorhamnetin-3-O-(2G-α-L-rhamnosyl)-rutinoside	C34H42O20	770.23	9.08	5368.00	829.24	3.9	+CH3COO	[M+H]-
	Isorhamnetin-3-O-(2G-α-L-rhamnosyl)-rutinoside	C34H42O20	770.23	10.77	4122.00	829.25	7.6	+CH3COO, +e	[M+H]-
	Isorhamnetin-3-gentiobioside-7-glucoside	C34H42O22	802.22	6.96	3306.00	837.18	-9.5	+Cl	[M+H]-
77	Polygalaside C	C35H44O19	768.25	7.72	10749.00	767.24	-3.5	-H, +HCOO	[M+H]-
	Polygalaside C	C35H44O19	768.25	8.79	81144.00	767.24	-2.0	-H, +Cl, +e, +HCOO	[M+H]-
78	(+)-Pinoresinol-β-D-glucopyranoside	C36H42O16	730.25	9.16	4805.00	765.22	8.1	+Cl	[M+H]-
79	2′,6′-Diacetyl-3,6-diferuloylsucrose	C36H42O19	778.23	10.15	4285.00	777.22	-2.0	-H, +HCOO	[M+H]-
80	Cistanoside A	C36H48O20	800.27	10.27	3213.00	835.25	5.1	+Cl	[M+H]-
81	Magnoflorine	C36H52O16	740.33	15.25	9823.00	799.34	-2.1	+CH3COO	[M+H]-
82	Platycogenic acid A lactone	C36H54O12	678.36	11.54	6809.00	677.35	-1.7	-H, +HCOO	[M+H]-
83	Phytolaccaside P	C36H56O12	680.38	11.83	126202.00	679.37	-1.0	-H, +Cl, +HCOO	[M+H]-
84	Neocuscutaside A	C37H46O21	826.25	9.81	41182.00	825.24	-1.9	-H	[M+H]-
85	1,2′,6′-Triacetyl-3,6-diferuloylsucrose	C38H44O20	820.24	11.63	8766.00	819.23	-2.5	-H	[M+H]-
86	Moracenin G	C40H36O11	692.23	9.10	9161.00	737.23	5.0	+HCOO	[M+H]-
87	1,2′,4′,6′-Tetraacetyl-3,6-diferuloylsucrose	C40H46O21	862.25	12.98	5887.00	861.24	-3.3	-H	[M+H]-
88	Triacetylaconitine	C40H53NO14	771.35	32.28	8623.00	816.35	6.4	+HCOO	[M+H]-
89	Lyciumin A	C42H51N9O12	873.37	14.81	18510.00	918.37	9.1	+HCOO	[M+H]-
90	Hookeroside D	C43H70O18	874.46	7.90	15527.00	873.45	-2.7	-H	[M+H]-
	Hookeroside D	C43H70O18	874.46	9.19	3442.00	873.45	-2.9	-H	[M+H]-
91	Ophiopogonin D	C44H70O16	854.47	7.13	3433.00	889.44	5.7	+Cl	[M+H]-
92	3-O-Tetradecanoyl-16-O-acetylisoiridogermanal	C46H78O6	726.58	34.57	3705.00	785.59	-3.7	+CH3COO	[M+H]-
93	Chikusetsusaponin Ib	C47H74O18	926.49	9.80	4832.00	971.48	-3.2	+HCOO	[M+H]-
94	Phytolaccaside I	C49H78O22	1018.50	9.80	16843.00	1017.49	-3.2	-H	[M+H]-
95	Stauntonoside YM13	C51H80O21	1028.52	11.00	7457.00	1073.51	-5.7	+HCOO	[M+H]-
	Cynanoside L	C52H80O23	1072.51	8.64	4326.00	1117.50	-3.9	+HCOO	[M+H]-
96	Cynanoside L	C52H80O23	1072.51	9.24	7204.00	1117.50	-4.1	+HCOO, +CH3COO	[M+H]-
	Cynanoside L	C52H80O23	1072.51	11.15	4293.00	1071.50	-4.5	-H	[M+H]-
97	Foetidissimoside A	C52H82O22	1058.53	10.20	497757.00	1103.52	-2.8	+HCOO	[M+H]-
98	Julibroside C1	C53H82O24	1102.52	10.11	14654.00	1101.51	-3.6	-H	[M+H]-

	Julibroside C1	C53H82O24	1102.52	10.77	7050.00	1101.51	-4.7	-H	$[M+H]^-$
99	Aster saponin Hc	C57H90O26	1190.57	10.04	107065.00	1235.57	-3.1	+HCOO	$[M+H]^-$
100	Timosaponin I2 (Timosaponin D2)	C57H96O28	1228.61	15.97	11855.00	1263.58	-2.4	+Cl	$[M+H]^-$
101	Timosaponin B-6	C58H98O29	1258.62	15.08	7983.00	1293.59	-2.3	+Cl	$[M+H]^-$
102	2″-O-Acetylpolygalacin D	C59H94O28	1250.59	10.38	93269.00	1249.58	-3.8	-H	$[M+H]^-$
103	Platycodin C	C59H94O29	1266.59	9.75	388427.00	1265.58	-3.0	-H	$[M+H]^-$
104	2-Hydroxyfuran-3-carboxylic acid	C5H4O4	128.01	38.52	4021.00	128.01	-4.1	+e	$[M+H]^-$
	Vaccaroside B	C60H94O29	1278.59	10.36	4894.00	1277.58	-4.4	-H	$[M+H]^-$
105	Vaccaroside B	C60H94O29	1278.59	14.12	3422.00	1323.60	8.0	+HCOO	$[M+H]^-$
	Vaccaroside B	C60H94O29	1278.59	15.42	27516.00	1323.60	7.1	+HCOO	$[M+H]^-$
106	Aster saponin Hd	C62H98O30	1322.61	9.97	51709.00	1367.61	-3.5	+HCOO	$[M+H]^-$
107	Tubeimoside II	C63H98O30	1334.61	10.27	99356.00	1379.61	-3.8	+HCOO	$[M+H]^-$
108	Tubeimoside III	C64H100O31	1364.62	15.13	105604.00	1409.63	7.2	+HCOO	$[M+H]^-$
109	Geniposidic acid tetramer	C64H82O37	1442.45	7.63	3017.00	1441.44	-4.3	-H	$[M+H]^-$
110	Lobatoside I	C65H102O33	1410.63	14.72	87248.00	1469.66	7.5	+CH3COO	$[M+H]^-$
111	2″-O-Acetylpolygalacin D2	C65H104O33	1412.65	9.97	32831.00	1411.63	-3.7	-H	$[M+H]^-$
	Geniposidic acid tetramer acetate	C66H84O38	1484.46	7.89	19607.00	1483.45	-4.0	-H, +HCOO	$[M+H]^-$
112	Geniposidic acid tetramer acetate	C66H84O38	1484.46	8.63	11445.00	1483.45	-3.5	-H, +Cl	$[M+H]^-$
	Geniposidic acid tetramer acetate	C66H84O38	1484.46	10.01	6515.00	1483.45	-4.7	-H, +HCOO	$[M+H]^-$
113	3-O-β-D-Galactopyranosyl-(1→2)-β-D-glucuronopyranosyl gypso-genin-28-O-β-D-xylopyranosyl-(1→4)-[β-D-6-O-acetyl glucopyranosyl-(1→3)]-α-L-rhamnopyranosyl-(1→2)-β-D-fucopyranoside	C67H104O34	1452.64	10.21	60196.00	1511.65	-3.7	+CH3COO	$[M+H]^-$
	3-O-β-D-Galactopyranosyl-(1→2)-β-D-glucuronopyranosyl gypso-genin-28-O-β-D-xylopyranosyl-(1→4)-[β-D-6-O-acetyl glucopyranosyl-(1→3)]-α-L-rhamnopyranosyl-(1→2)-β-D-fucopyranoside	C67H104O34	1452.64	15.36	11965.00	1497.65	5.5	+HCOO, +CH3COO	$[M+H]^-$
114	Parthenocissin A	C68H52O44	1572.18	14.45	25905.00	1572.19	2.5	+e, -H	$[M+H]^-$
	Parthenocissin A	C68H52O44	1572.18	14.78	4592.00	1631.20	3.2	+CH3COO	$[M+H]^-$
115	Platycoside D	C69H112O37	1532.69	14.01	5851.00	1591.69	-6.8	+CH3COO	$[M+H]^-$
116	(2R,3R,4R,5S)-2-(Hydroxymethyl)-3,4,5-trihydroxypiperidine	C6H13NO4	163.08	0.64	3222.00	198.05	-6.8	+Cl	$[M+H]^-$
	Polygalacin G	C70H104O32	1456.65	13.18	4447.00	1456.64	-7.5	+e	$[M+H]^-$
117	Polygalacin G	C70H104O32	1456.65	13.69	24580.00	1455.64	-3.9	-H, +HCOO	$[M+H]^-$
	Polygalacin G	C70H104O32	1456.65	14.41	31745.00	1455.64	-3.1	-H	$[M+H]^-$
	Polygalacin G	C70H104O32	1456.65	15.02	140019.00	1455.64	-3.0	-H	$[M+H]^-$

118	3-O-β-D-Galactopyranosyl-(1→2)-β-D-glucuronopyranosyl-(1→3)-β-D-glucuronopyranosylgypsogenin-28-O-β-D-xylopyranosyl-(1→4)-[β-D-glucopyranosyl-(1→3)]-α-L-rhamnopyranosyl-(1→2)-β-D-fucopyranoside	C70H110O37	1542.67	9.81	31652.00	1541.66	-3.9	-H	$[M+H]^-$
	3-O-β-D-Galactopyranosyl-(1→2)-β-D-glucuronopyranosyl-(1→3)-β-D-glucuronopyranosylgypsogenin-28-O-β-D-xylopyranosyl-(1→4)-[β-D-glucopyranosyl-(1→3)]-α-L-rhamnopyranosyl-(1→2)-β-D-fucopyranoside	C70H110O37	1542.67	13.83	56983.00	1601.69	5.0	+CH3COO	$[M+H]^-$
	3-O-β-D-Galactopyranosyl-(1→2)-β-D-glucuronopyranosyl-(1→3)-β-D-glucuronopyranosylgypsogenin-28-O-β-D-xylopyranosyl-(1→4)-[β-D-glucopyranosyl-(1→3)]-α-L-rhamnopyranosyl-(1→2)-β-D-fucopyranoside	C70H110O37	1542.67	14.63	69843.00	1541.68	6.9	-H	$[M+H]^-$
	3-O-β-D-Galactopyranosyl-(1→2)-β-D-glucuronopyranosyl-(1→3)-β-D-glucuronopyranosylgypsogenin-28-O-β-D-xylopyranosyl-(1→4)-[β-D-glucopyranosyl-(1→3)]-α-L-rhamnopyranosyl-(1→2)-β-D-fucopyranoside	C70H110O37	1542.67	15.30	11220.00	1541.67	4.8	-H	$[M+H]^-$
119	Polygalacin E	C71H106O33	1486.66	13.55	20385.00	1485.65	-4.1	-H	$[M+H]^-$
	Polygalacin E	C71H106O33	1486.66	14.84	84843.00	1485.65	-2.9	-H	$[M+H]^-$
120	Gleditsioside J	C74H120O39	1632.74	14.03	5091.00	1667.72	3.3	+Cl	$[M+H]^-$
121	Polygalacin B	C75H112O35	1572.70	13.10	141319.00	1617.69	-4.0	+HCOO	$[M+H]^-$
	Polygalacin B	C75H112O35	1572.70	14.14	254215.00	1631.71	-3.0	+CH3COO	$[M+H]^-$
	Polygalacin B	C75H112O35	1572.70	14.46	468116.00	1571.69	-2.7	-H, +HCOO	$[M+H]^-$
122	Polygalacin F	C75H112O36	1588.69	12.87	4125.00	1587.68	-5.1	-H	$[M+H]^-$
	Polygalacin F	C75H112O36	1588.69	13.73	14370.00	1647.70	-4.5	+CH3COO	$[M+H]^-$
	Polygalacin F	C75H112O36	1588.69	14.02	134681.00	1587.68	-2.9	-H	$[M+H]^-$
	Polygalacin F	C75H112O36	1588.69	15.01	256636.00	1587.68	-3.2	-H	$[M+H]^-$
123	Polygalacin A	C80H120O39	1704.74	13.93	244588.00	1703.73	-3.1	-H	$[M+H]^-$
	Polygalacin A	C80H120O39	1704.74	14.15	163327.00	1749.73	-3.5	+HCOO	$[M+H]^-$
	Polygalacin A	C80H120O39	1704.74	14.89	6354.00	1749.73	-5.1	+HCOO	$[M+H]^-$

References

1. Chinese Pharmacopoeia Commission, 2025. Pharmacopoeia of the People's Republic of China. Volume 1, 54-55.

2. Tian J X, Xie Y S, Li J Y, Pei Z H, Jiang K, Zhao J Y, Wu P, 2024. Re-examination of Strychni Semen in Ancient Materia-Medica Literature and Advances in Its Efficacy and Clinical Applications. Journal of Chinese Medicinal Materials. 47(6), 1566-1573.
3. QIN B B, JIA Z F, WANG J L, MA L, ZHANG T J, HU J, 2022. Research progress on chemical components and pharmacological effects of Strychni Semen and prediction and analysis of its quality markers. 53(18), 5920-5933.
4. Chen S Y, Ma N, Xu Y Y, Li Y B, 2023. Research progress on target organ toxicity and attenuation and synergistic mechanism of Strychni Semen. Drugs & Clinic. 38(3), 725-730.
5. Song H B, Du X X, 2015. Literature Study on Adverse Reactions of Strychni Semen and Analysis of Risk Factors. Chinese Journal of Pharmacovigilance. 12(7), 411-416.
6. Zhang Q G, Zhang Q X, Zhang Y. 2012. Advances in Pharmacology, Toxicology and Safety Evaluation of Strychni Semen. Mod Diagn Treat. 23(9), 1422-1423.
7. Qin C C, Du Q Y, Zang Y M, Sun M L, Zhang Z H, Wang J F, 2024. Historical evolution and modern research progress of processing Strychni Semen. China Journal of Traditional Chinese Medicine and Pharmacy. 39(1), 319-325.
8. Chatripakon S, Mabon L L, 2003. Strychnine-sensitive glycine receptors depress hyperexcitability in rat dentate gyrus. J Neurophysiol. 89(3), 1339.
9. Akaike N, Kaneda M, 1989. Glycine gated chloride current in acutely isolated rat hy pothalamic neurons. J Neurophysiol. 62(6), 1400.
10. Paul Petrus, Marlene Cervantes, Muntaha Samad, Tomoki Sato, Alina Chao, Shogo Sato, Kevin B. Koronowski, Grace Park, Yasmine Alam, Niklas Mejhert, Marcus M. Seldin, José Manuel Monroy Kuhn, Kenneth A. Dyar, Dominik Lutter, Pierre Baldi, Peter Kaiser, Cholsoon Jang, Paolo Sassone-Corsi, 2022. Tryptophan metabolism is a physiological integrator regulating circadian rhythms. Molecular Metabolism, DOI: 10.1016/j.molmet.2022.101556.
11. Wonodi, I.; Stine, O.C.; Sathyasaikumar, K.V.; Roberts, R.C.; Mitchell, B.D.; Hong, L.E.; Kajii, Y.; Thaker, G.K.; Schwarcz, R. Downregulated kynurenine 3-monooxygenase gene expression and enzyme activity in schizophrenia and genetic association with schizophrenia endophenotypes. Arch. Gen. Psychiatry 2011, 68, 665–674.
12. Milan Holecek, 2026. Serotonin, Kynurenine, and Indole Pathways of Tryptophan Metabolism in Humans in Health and Disease. Nutrients. 18(3).
13. Yuechang Wang, Yonggang Zhang, Wei Wang, Yanmin Zhang, Xueqian Dong, Yang Liu, 2025. Diverse Physiological Roles of Kynurenine Pathway Metabolites: Updated Implications for Health and Disease. metabolites. 15, 210.
14. Makoto Fujikawa, Masashi Ueda, Kenta Maruyama, 2024. Role of Kynurenine and Its Derivatives in the Neuroimmune System. International Joumal of Molecular Sciences. 25, 7144.
15. Igor Cervenka, Leandro Z. Agudelo, Jorge L, Ruas, 2017. Kynurenines: Tryptophan's metabolites in exercise, inflammation, and mental health. Science, 357(6349): eaaf9794.
16. Pengbo Yang, Junhua Zhang, 2023. Indoleamine 2,3-Dioxygenase (IDO) Activity: A Perspective Biomarker for Laboratory Determination in Tumor Immunotherapy. Biomedicines, DOI: 10.3390/biomedicines11071988.
17. Kanai M, Funakoshi H, Takahashi H, Hayakawa T, Mizuno S, Matsumoto K, Nakamura T, 2009. Tryptophan 2,3-dioxygenase is a key modulator of physiological neurogenesis and anxiety-related behavior in mice. Molecular Brain, 2, 8. DOI: 10.1186/1756-6606-2-8
18. Stone T W, Darlington L G, Badawy A A, Williams R O, 2024. The Complex World of Kynurenic Acid: Reflections on Biological Issues and Therapeutic Strategy. International Journal of Molecular Sciences, 25(16): 9040. DOI: 10.3390/ijms25169040.
19. Leqing Xu, Zhao Zhao, Yufei Zhang, Chunlai Ma, 2025. The interplay between metabolism and neuroinflammation in epilepsy: mechanisms and therapeutic perspectives. Journal of Neuroinflammation, DOI: 10.1186/s12974-025-03553-w.
20. Ana Pocivavsek, Sophie Erhardt, 2023. Kynurenic acid: translational perspectives of a therapeutically targetable gliotransmitter. Neuropsychopharmacology, 48(13): 2029-2038. DOI: 10.1038/s41386-023-01681-6.
21. Guillemin G J, Kerr S J, Smythe G A, Smith D G, Kapoor V, Armati P J, Croitoru J, Brew B J, 2001. Kynurenine pathway metabolism in human astrocytes: A paradox for neuronal protection. Journal of Neurochemistry. 78, 842–853.
22. Korrapati V. Sathyasaikumar, Verónica Pérez de la Cruz, Benjamín Pineda, Gustavo Ignacio Vázquez Cervantes, Daniela Ramírez Ortega, David W. Donley, Paul L. Severson, Brian L. West, Flaviano Giorgini, Jonathan H. Fox, Robert Schwarcz, 2022. Cellular Localization of Kynurenine 3-Monooxygenase in the Brain: Challenging the Dogma. Antioxidants, 11, 315. DOI: 10.3390/antiox11020315.

23. Jiang, Z.; Liu, D.; Li, T.; Gai, C.; Xin, D.; Zhao, Y.; Song, Y.; Cheng, Y.; Li, T.; Wang, Z. Hydrogen sulfide reduces oxidative stress in Huntington's disease via Nrf2. Neural Regen. Res. 2025, 20, 1776–1788.
24. Madella, A.M.; Van Bergenhenegouwen, J.; Garssen, J.; Masereeuw, R.; Overbeek, S.A. Microbial-Derived Tryptophan Catabolites, Kidney Disease and Gut Inflammation. Toxins 2022, 14, 645.
25. Guillemin
26. Hestad K, Alexander, J.; Rootwelt, H.; Aaseth, J.O. The Role of Tryptophan Dysmetabolism and Quinolinic Acid in Depressive and Neurodegenerative Diseases. Biomolecules 2022, 12, 998. [CrossRef]
27. Kubicova, L.; Hadacek, F.; Weckwerth, W.; Chobot, V. Effects of endogenous neurotoxin quinolinic acid on reactive oxygen species production by Fenton reaction catalyzed by iron or copper. J. Organomet. Chem. 2015, 782, 111–115.
28. Li, D.; Yu, S.; Long, Y.; Shi, A.; Deng, J.; Ma, Y.; Wen, J.; Li, X.Q.; Liu, S.Y.; Zhang, Y.L.; et al. Tryptophan metabolism: Mechanism-oriented therapy for neurological and psychiatric disorders. Front. Immunol. 2022, 13, 985378.
29. Hansen, K.B.; Yi, F.; Perszyk, R.E.; Menniti, F.S.; Traynelis, S.F. NMDA Receptors in the Central Nervous System. Methods Mol. Biol. 2017, 1677, 1–80.
30. Rahman, A.; Rao, M.S.; Khan, K.M. Intraventricular infusion of quinolinic acid impairs spatial learning and memory in young rats: A novel mechanism of lead-induced neurotoxicity. J. Neuroinflamm. 2018, 15, 263. [CrossRef] [PubMed]
31. Morrens, M.; Coppens, V.; Walther, S. Do Immune Dysregulations and Oxidative Damage Drive Mood and Psychotic Disorders? Neuropsychobiology 2020, 79, 251–254. [CrossRef]
32. Loganathan, C.; Thayumanavan, P. Asiatic acid prevents the quinolinic acid-induced oxidative stress and cognitive impairment. Metab. Brain Dis. 2018, 33, 151–159. [CrossRef]
33. Nowicka-St ˛azka, P.; Langner, E.; Turski, W.; Rzeski, W.; Parada-Turska, J. Quinaldic acid in synovial fluid of patients with ˙rheumatoid arthritis and osteoarthritis and its effect on synoviocytes in vitro. Pharmacol. Rep. 2018, 70, 277–283.
34. Nakamura, K.; Sugawara, Y.; Sawabe, K.; Ohashi, A.; Tsurui, H.; Xiu, Y.; Ohtsuji, M.; Lin, Q.S.; Nishimura, H.; Hasegawa, H.;et al. Late developmental stage-specific role of tryptophan hydroxylase 1 in brain serotonin levels. J. Neurosci. 2006, 26, 530–534.
35. Hannon, J.; Hoyer, D. Molecular biology of 5-HT receptors. Behav. Brain Res. 2008, 195, 198–213. [CrossRef]
36. Oh, C.M.; Namkung, J.; Go, Y.; Shong, K.E.; Kim, K.; Kim, H.; Park, B.Y.; Lee, H.W.; Jeon, Y.H.; Song, J.; et al. Regulation of systemic energy homeostasis by serotonin in adipose tissues. Nat. Commun. 2015, 6, 6794. [CrossRef]
37. Bader, M. Inhibition of serotonin synthesis: A novel therapeutic paradigm. Pharmacol. Ther. 2020, 205, 107423. [CrossRef]
38. Jones, L.A.; Sun, E.W.; Martin, A.M.; Keating, D.J. The ever-changing roles of serotonin. Int. J. Biochem. Cell Biol. 2020, 125, 105776.
39. Hanan Alkozi, Maria Perez de Lara, Juan Sánchez-Naves, Jesús Pintor, 2017. TRPV4 Stimulation Induced Melatonin Secretion by Increasing Arylalkymine N-acetyltransferase (AANAT) Protein Level. International Journal of Molecular Sciences. DOI: 10.3390/ijms18040746
40. Palmer, E.E.; Leffler, M.; Rogers, C.; Shaw, M.; Carroll, R.; Earl, J.; Cheung, N.W.; Champion, B.; Hu, H.; Haas, S.A.; et al. New insights into Brunner syndrome and potential for targeted therapy. Clin. Genet. 2016, 89, 120–127.
41. Andrani, M.; Dall'Olio, E.; De Rensis, F.; Tummaruk, P.; Saleri, R. Bioactive Peptides in Dairy Milk: Highlighting the Role of Melatonin. Biomolecules 2024, 14, 934.
42. Fadda, F. Tryptophan-Free Diets: A Physiological Tool to Study Brain Serotonin Function. News Physiol. Sci. 2000, 15, 260–264.
43. Hardeland, R. Melatonin metabolism in the central nervous system. Curr. Neuropharmacol. 2010, 8, 168–181.
44. Tan, D.X.; Reiter, R.J.; Manchester, L.C.; Yan, M.T.; El-Sawi, M.; Sainz, R.M.; Mayo, J.C.; Kohen, R.; Allegra, M.; Hardeland, R. Chemical and physical properties and potential mechanisms: Melatonin as a broad spectrum antioxidant and free radical scavenger. Curr. Top. Med. Chem. 2002, 2, 181–197.